creative commons
COMMONS DEED

저작자표시-비영리-변경금지 2.0 대한민국

이용자는 아래의 조건을 따르는 경우에 한하여 자유롭게

- 이 저작물을 복제, 배포, 전송, 전시, 공연 및 방송할 수 있습니다.

다음과 같은 조건을 따라야 합니다:

저작자표시. 귀하는 원저작자를 표시하여야 합니다.

비영리. 귀하는 이 저작물을 영리 목적으로 이용할 수 없습니다.

변경금지. 귀하는 이 저작물을 개작, 변형 또는 가공할 수 없습니다.

- 귀하는, 이 저작물의 재이용이나 배포의 경우, 이 저작물에 적용된 이용허락조건을 명확하게 나타내어야 합니다.
- 저작권자로부터 별도의 허가를 받으면 이러한 조건들은 적용되지 않습니다.

저작권법에 따른 이용자의 권리는 위의 내용에 의하여 영향을 받지 않습니다.

이것은 이용허락규약(Legal Code)을 이해하기 쉽게 요약한 것입니다.

Disclaimer

dCollection

ULSAN NATIONAL INSTITUTE OF SCIENCE AND TECHNOLOGY

Master`s Thesis

Design of a multi-layer electrolyte cell using $Li_{1.3}Ti_{1.7}Al_{0.3}(PO_4)_3$ ceramic electrolyte material

Seongwoo Heo

Department of Energy Engineering

(Battery Science and Technology)

Graduate School of UNIST

2017

ULSAN NATIONAL INSTITUTE OF
SCIENCE AND TECHNOLOGY

Design of a multi-layer electrolyte cell using $Li_{1.3}Ti_{1.7}Al_{0.3}(PO_4)_3$ ceramic electrolyte material

Seongwoo Heo

Department of Energy Engineering

(Battery Science and Technology)

Graduate School of UNIST

ULSAN NATIONAL INSTITUTE OF
SCIENCE AND TECHNOLOGY

Design of a multi-layer electrolyte cell using $Li_{1.3}Ti_{1.7}Al_{0.3}(PO_4)_3$ ceramic electrolyte material

A thesis/dissertation

submitted to the Graduate School of UNIST

in partial fulfillment of the

requirements for the degree of

Master of Science

Seongwoo Heo

07.13.2017

Approved by

Advisor

Youngsik Kim

ULSAN NATIONAL INSTITUTE OF SCIENCE AND TECHNOLOGY

Design of a multi-layer electrolyte cell using $Li_{1.3}Ti_{1.7}Al_{0.3}(PO_4)_3$ ceramic electrolyte material

Seongwoo Heo

This certifies that the thesis/dissertation of Seongwoo Heo is approved.

07. 13. 2017

signature

Advisor: Youngsik Kim

signature

Yoonseok Jung

signature

Seokju Kang

ULSAN NATIONAL INSTITUTE OF SCIENCE AND TECHNOLOGY

Contents

ULSAN NATIONAL INSTITUTE OF SCIENCE AND TECHNOLOGY

Abstract

Energy storage systems have been developed to satisfy the demand of energy density for electric vehicles and large-scale ESS plants. The electrochemical stability window of commercial carbonate-base electrolytes is from cathodic limit 0.8V to anodic limit 4.3V vs. Li/Li^+. The oxidation decomposition of carbonate electrolytes prevents realization of 5.0V-class high voltage of Li-ion battery (LIB) because of problems such as capacity fading by decomposition of electrolytes and the Mn-dissolution of cathodes.

In this thesis, Multi-layer electrolyte cell (MEC) has improved the electrochemical high voltage stability and thermal stability by introducing an ionic liquid electrolyte as the cathode-side electrolyte. The ionic liquid electrolyte has high electrochemical stability for high potential oxidative reaction compared to a carbonate-base electrolyte and thermal stability. The first MEC model has improved the stability of high potential and elevated temperature, but it has low reversible capacity compared to commercial electrolyte coin-cell. This is caused by the polarization losses: 1) activation polarization, 2) concentration polarization and 3) Ohmic polarization.

The Ohmic polarization is caused by the ionic conductivity of the electrolyte, electronic resistance of the active materials and current collectors and the interfacial resistance between them. MEC has high internal resistance of multi-layer electrolyte because the ionic liquid electrolyte and ceramic electrolyte pellet have interfacial resistance between them. We expanded the contact surface with porous LTAP pellet and ionic liquid to reduce the internal resistance of MEC. The porous type MEC has enhanced reversible capacity and good stability for high potential and temperature at low C-rate. MEC designs have intrinsic high internal resistance compared to commercial LIB, so the composition electrolyte of MEC should be develop their ionic conductivity and good interfacial resistance.

ULSAN NATIONAL INSTITUTE OF SCIENCE AND TECHNOLOGY

The graphite anode forms the SEI layer (Solid electrolyte interphase) consuming the reversible lithium ion in LIB because the electrochemical stability window of the electrolyte is higher than the redox potential of graphite. The ceramic electrolyte $Li_{1.3}Ti_{1.7}Al_{0.3}(PO_4)_3$ (LTAP) materials could provide an additional lithium source to recover the capacity of LIB full-cell. They have NASICON – type structure of two Li sites M1, M2. The M1 site is occupied by existing Li^+ ion, additional Li^+ ions can be inserted into the vacant M2 site. After the first charge cycle, LTAP has ionic conductivity 10^{-4} S/cm, so it helps lithium ion conduct inside the cell. LTAP materials provide an additional lithium source about 110 mAh/g. The contribution of lithium source material is confirmed by applying to graphite / $LiCoO_2$ full-cell. To achieve higher capacity, ceramic electrolyte materials that have higher capacity could be applied.

ULSAN NATIONAL INSTITUTE OF SCIENCE AND TECHNOLOGY

List of figures

ULSAN NATIONAL INSTITUTE OF SCIENCE AND TECHNOLOGY

$Li_{1.2}Ni_{0.15}Mn_{0.55}Co_{0.1}O_2$ at C/10 rate and 55`C.

Figure 1.15 (a) Charge and discharge voltage profile for a Multi-layer electrolyte cell (1.0M $LiPF_6$ in EC:DMC (1:1vol/vol%) / S.E. / 0.1mol% LiTFSI in $Py_{14}TFSI$) of Li / $Li_{1.2}Ni_{0.15}Mn_{0.55}Co_{0.1}O_2$ at C/30 rate and 55`C (b) polarization effect on voltage variation (c) electrochemical impedance spectroscopy for Multi-layer electrolyte cell.

Figure 1.16 Electrochemical impedance spectroscopy for Multi-layer electrolyte cell (1.0M $LiPF_6$ in EC:DMC (1:1vol/vol) / Solid electrolyte / 0.1mol% LiTFSI in $Py_{14}TFSI$) without active material.

Figure 1.17 Voltage profile for Multi-layer electrolyte cell (1.0M $LiPF_6$ in EC:DMC (1:1vol/vol%) / S.E. / 0.1mol% LiTFSI in $Py_{14}TFSI$) cycling (a) Li / $LiCoO_2$ half-cell, (b) Li / $LiFePO_4$ half-cell at room temperature.

Figure 1.18 (a) Thermogravimetric analysis of mixture pellet of LTAP powder and precursors and (b) density examination of synthesized porous LTAP pellet (c) SEM images of OHARA LTAP pellet and porous LTAP pellet.

Figure 1.19 (a) Electrochemical impedance spectroscopy for three type multi-layer electrolyte cells of Li / $Li_{1.2}Ni_{0.15}Mn_{0.55}Co_{0.1}O_2$ (b) schematic ion conducting pathway throughout multi-layer electrolyte cell.

Figure 1.20 Charge and discharge voltage profile for porous pellet type multi-layer electrolyte cell (1.0M $LiPF_6$ in EC:DMC (1:1vol/vol%) / S.E. / 0.1mol% LiTFSI in $Py_{14}TFSI$) of Li / $Li_{1.2}Ni_{0.15}Mn_{0.55}Co_{0.1}O_2$ at C/20 rate and 55`C.

Figure 1.21 Charge and discharge voltage profile for ionic liquid electrolyte half-cell ($Py_{14}TFSI$) of Li / $Li_{1.2}Ni_{0.15}Mn_{0.55}Co_{0.1}O_2$ at C/20 rate and 55`C.

Figure 2.1 (a) SEI layer formation consumes the Li ion causing dead volume of the cathode materials (b) reduction of the capacity limited in full-cell by SEI layer formation (c) Lithium source additives compensate the capacity consumed by SEI layer formation, which leading the cathode materials utilized at the max (d) lithium source additive candidates and conditions for the additive.

Figure 2.2 (a) Voltage profile showing the capacity, redox potential and stability of the lithium source additive at high voltage (b) Schematic of their corresponding energy vs. density of states describing Li^+ ions contribution and the stability of the candidate at high voltage.

ULSAN NATIONAL INSTITUTE OF SCIENCE AND TECHNOLOGY

Figure 2.3 Preparation of lithium source material $Li_{1.3+1.7}Ti_{1.7}Al_{0.3}(PO_4)_3$

Figure 2.4 (a) Powder X-ray diffraction pattern of the $Li_{1.3}Ti_{1.7}Al_{0.3}(PO_4)_3$, $Li_{1.3+1.7}Ti_{1.7}Al_{0.3}(PO_4)_3$, mixed powder LCO with Li rich LTAP (b) SEM image of the ground $Li_{1.3}Ti_{1.7}Al_{0.3}(PO_4)_3$ (c) crystal NASICON – type structure of $Li_{1.3}Ti_{1.7}Al_{0.3}(PO_4)_3$**.**

Figure 2.5 Ionic conductivity of (a) lithium source additive $Li_{1.3+1.7}Ti_{1.7}Al_{0.3}(PO_4)_3$ (b) electrochemical charge/discharge voltage profile of Li / $Li_{1.3+1.7}Ti_{1.7}Al_{0.3}(PO_4)_3$ half-cell.

Figure 2.6 (a), (b) Initial full cell cycle performance of pristine and the mixed $Li_{1.3+1.7}Ti_{1.7}Al_{0.3}(PO_4)_3$ with $LiCoO_2$ cathode at C/20 rate (c) subsequent cycle of them at C/10 rate. The anode is the graphite (d) The corresponding charge/discharge performances cycled at C/20 for initial two cycles and C/10 for the subsequence cycles.

ULSAN NATIONAL INSTITUTE OF
SCIENCE AND TECHNOLOGY

List of tables

ULSAN NATIONAL INSTITUTE OF SCIENCE AND TECHNOLOGY

Chapter 1

1. Multi-layer electrolyte cell for stabilizing high voltage cathode material

1.1 Introduction to rechargeable Li ion batteries

The magnitude of the global energy market has been increased during several decades. People rely heavily on traditional fuels such as gasoline and natural gas and nuclear power plants to meet global energy demands. The consumption of fossil fuels has increased the release of greenhouse gases in the air, which causes abnormal weather phenomena like global warming. Although nuclear power generation has high energy density, it has great disadvantages of radioactive pollution waste. Engineers and researchers have instituted renewable energy plants to reduce dependence on traditional fuels and nuclear power. However, it is difficult to match the energy demand with renewable energy generation. Instead, energy storage systems (ESS) have been introduced to recover the energy deficiency when the energy demand exceeds the generation of renewable energy. One storage facility has a capacity between 100 kW and more than 100 MW [1].

Portable electric devices like mobile phones, laptop computers and electric vehicles (EV) as well as bulk ESS have been spotlighted world widely. EVs require an energy density more than one hundred times larger as that of other devices. People have designated the target for higher energy density than the current density of 140 Wh/kg, the distance 160 km covered. Li^+ ion has high specific coulombic charge except for hydrogen compared to other elements and Li-ion batteries (LIB) could provide high energy density as shown in Table 1. Researchers have investigated many materials to increase the energy density of LIB.

ULSAN NATIONAL INSTITUTE OF SCIENCE AND TECHNOLOGY

System	**Lithium Ion**	**Nickel Metal-Hydride**	**Lead Acid**	**Nickel-Cadmium**	**Zinc / air**
Anode	Carbon (Graphite)	Metal-Hydride	Lead Alloy	Cadmium	Zn
Cathode	$LiCoO_2$	Nickel oxyhydroxide	Lead dioxide	Nickel oxyhydroxide	O2 (air)
Electrolyte	Organic solvent, salt solution	Aqueous KOH, polypropylene	Aqueous H_2SO_4, polyethylene	Aqueous KOH, polypropylene	Aqueous KOH
Nominal voltage (V)	3.6	-	2	-	-
Energy density (Wh/ L)	260	220	70	60-100	200
Power Density (W/L)	400-500	475	~400	220-360	190
Cycle Life	500-1000	300-600	250-500	300-700	~200

Table 1. Major rechargeable batteries characteristics [2].

The 4.0V LIB has been developed since Prof. John B. Goodenough demonstrated $LiCoO_2$ layered structure in 1979. SONY company commercialized rechargeable lithium ion battery graphite / $LiCoO_2$ in 1990. The commercialized lithium ion battery is composed of lithium cobalt oxide cathode, graphite anode, carbonate-based electrolyte and polyolefin separator in figure 1.1. Cathode and anode materials decide the energy density of the LIB, while the polyolefin separator prevents short-circuits between the cathode and anode. The role of electrolyte is to deliver the solvated Li^+ ion to each electrode during charging or discharging process, so it balances the charge of electron with Li^+ ion inside the battery.

An electrochemical cell operate within an electrochemical stability window of the electrolyte in figure 1.2[3]. The electrochemical stability window is the energy level interval between the highest occupied molecular orbital (HOMO) level and the lowest unoccupied molecular orbital (LUMO) level of the electrolyte molecule, which is the voltage range between which the

ULSAN NATIONAL INSTITUTE OF SCIENCE AND TECHNOLOGY

substance is neither oxidized nor reduced. The cathode and anode materials are able to have reversible redox couple reaction without any side reactions of the electrolyte inside this window.

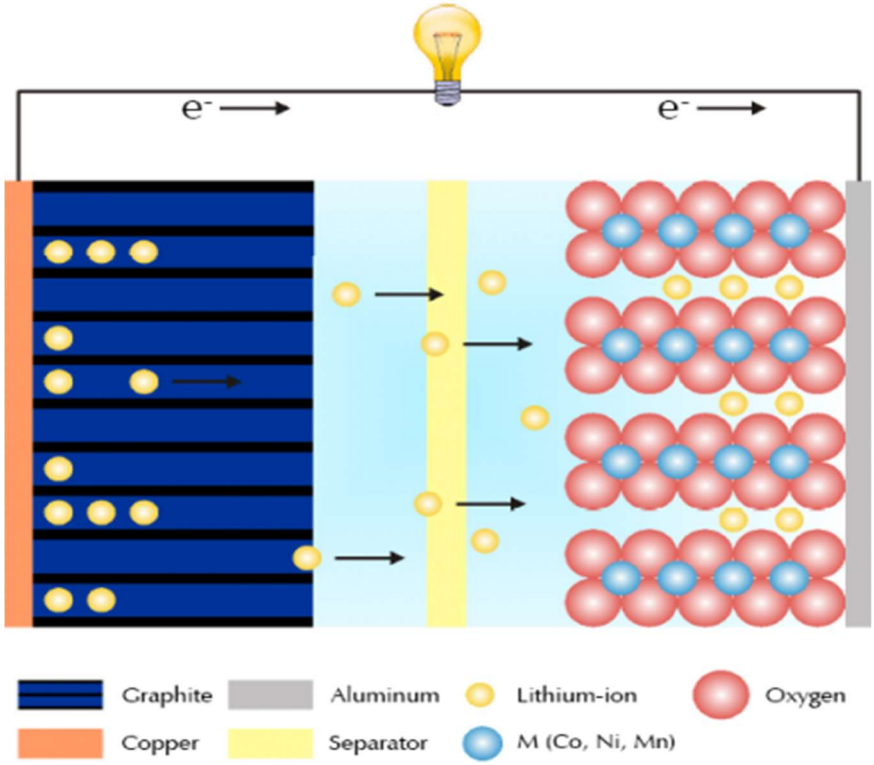

Figure 1.1 Li ion batteries system components.

The commercialized electrolyte has the electrochemical stability window from cathodic limit 0.8V to anodic limit 4.3V vs. Li/Li^+. The cathode materials $LiCoO_2$, $LiFePO_4$ has the redox couple potential 4.0V, 3.5V vs. Li/Li^+ respectively. However, it is necessary to research higher potential materials than these materials to meet the increasing demand for energy density. The investigation of high potential materials should be developed with the research of an electrolyte that is stable at high potential. The multi-layer electrolyte cell is designed to develop the stable electrolyte at high voltage in this chapter.

ULSAN NATIONAL INSTITUTE OF SCIENCE AND TECHNOLOGY

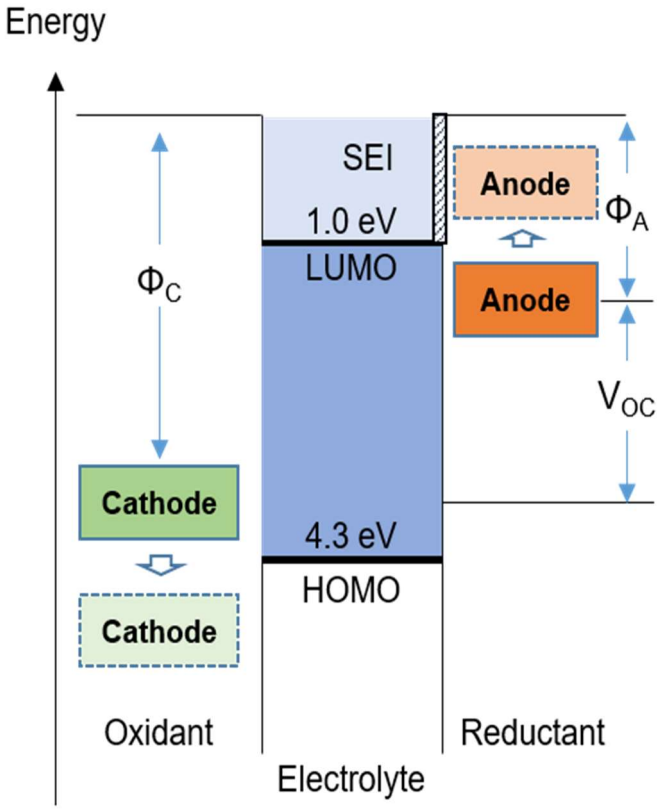

Figure 1.2 Electrochemical potential diagram of electrodes materials and electrolytes [3].

The potential of the graphite anode exceeds the electrochemical stability window of the electrolyte. The graphite anode forms a solid electrolyte interphase layer (SEI layer) during the decomposition of the electrolyte. This SEI layer insulates the graphite anode from the electrolyte and is permeable to lithium ion, so it prevents further decomposition of the electrolyte during cycle. The ideal SEI layer remains stable during cycle. However, it is broken down and reconstructed repeatedly. The formation of the SEI layer consumes the reversible lithium ion, which means that the reversible capacity of the LIB decreases. The breakdown of SEI layer is accelerated in harsh conditions such as elevated temperatures. An inorganic solid electrolyte as lithium ion additive that could recover the reversible capacity is introduced in chapter 2.

ULSAN NATIONAL INSTITUTE OF SCIENCE AND TECHNOLOGY

1.2 Multi-layer electrolyte cell for high voltage cathode material

5.0V-class spinel $LiNi_{0.5}Mn_{1.5}O_4$ cathode materials have high redox potential of 4.7V vs. Li/Li^+ and it has a reasonably high theoretical capacity of 147 $mAhg^{-1}$ shown as figure 1.3[3], so has become a promising candidate for the realization of a high energy density LIB. However, some critical drawbacks for the commercialization of $LiNi_{0.5}Mn_{1.5}O_4$ for LIB application are that oxidative decomposition at the $LiNi_{0.5}Mn_{1.5}O_4$ – electrolyte interfaces occur because of the low anodic limit of the commercial carbonate-based electrolytes, around 4.3V vs. Li/Li^+. Second, spinel $LiNi_{0.5}Mn_{1.5}O_4$ causes the "Mn dissolution" problem that reduces the cyclability of full-cells with graphite anode critically.

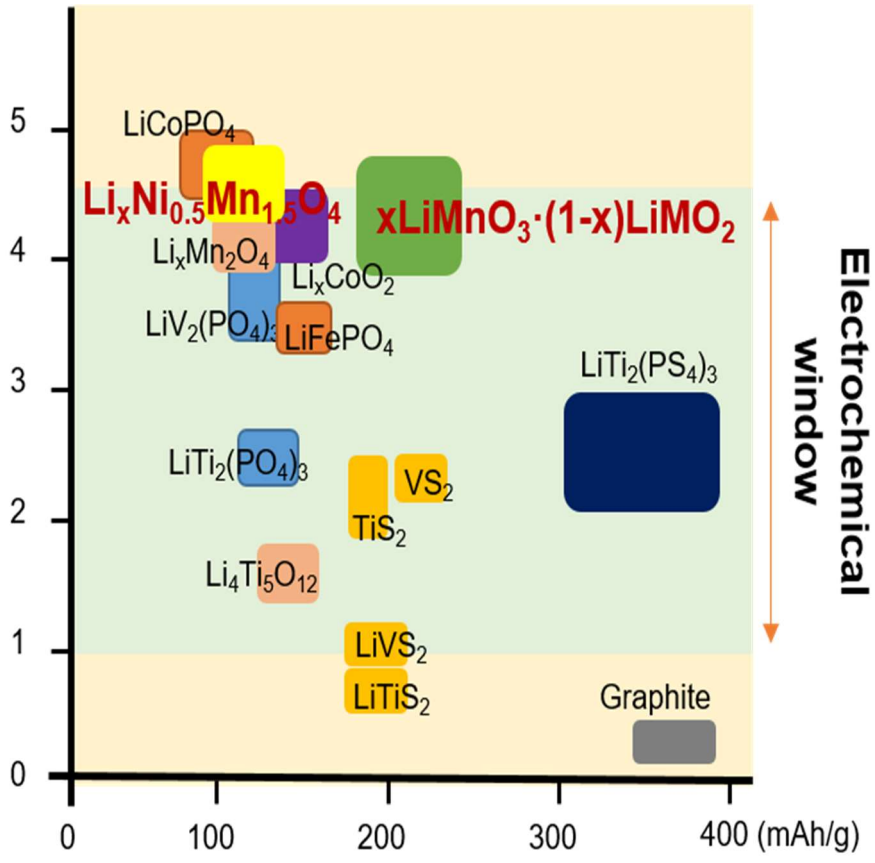

Figure 1.3 Schematic representation potential vs. capacity of Li-ion battery electrode materials [3].

ULSAN NATIONAL INSTITUTE OF SCIENCE AND TECHNOLOGY

The Mn dissolution reaction mechanisms are shown in figure 1.4. There are two possible Mn dissolution mechanisms ($2Mn^{3+}_{solid} \rightarrow Mn^{4+}_{solid} + Mn^{2+}_{solution}$). A trace of water in cell components such as electrode surfaces, separator and electrolyte can accelerate the undesirable side reaction with $LiPF_6$ in the electrolyte followed by a series of reactions[4,5,6].

$$LiPF_6 \leftrightarrow LiF(s) + PF_5$$

$$PF_5 + H_2O \leftrightarrow POF_3 + 2HF$$

$$POF_3 + H_2O \leftrightarrow PO_2F_2H + HF$$

$$PO_2F_2H + H_2O \leftrightarrow PO_3FH_2 + HF$$

$$PO_3FH_2 + H_2O \leftrightarrow PO_4H_3 + HF$$

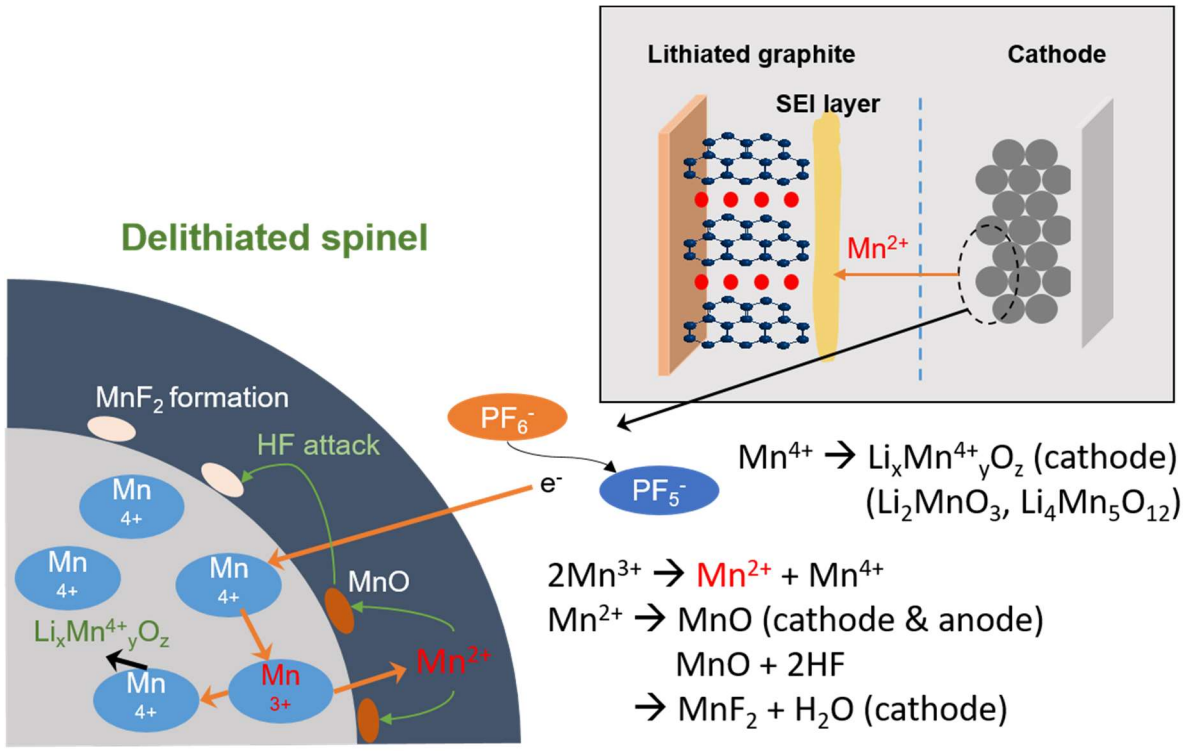

Figure 1.4 Mn dissolution reaction mechanism of spinel structure [4].

H^+ ions in HF react with $LiMn_2O_4$ to degrade into MnO and MnO_2 according to $2LiMn_2O_4 + 4H^+ \rightarrow 3MnO_2 + MnO + Li_2O + 2H_2O$[7]. The other is the HF attack to $LiMn_2O_4$ structure[8].

ULSAN NATIONAL INSTITUTE OF SCIENCE AND TECHNOLOGY

MnF_2 formation is according to the following reaction[8] :

$$2LiMn_2O_4 + 4H^+ + 4F^- \rightarrow 3MnO_2\ MnF_2 + 2LiF + 2H_2O$$

In harsh conditions of high potential and elevated temperatures, PF^{6-} anions tend to degrade to PF^{5-}, and subsequently Mn^{4+} ions are easier to reduce to Mn^{3+}, as follows:

$$LiPF^6 \rightarrow PF^5 + e^-$$

$$Mn^{4+} + e^- \rightarrow Mn^{3+}$$

The result is that the problem of Mn dissolution is often activated at elevated temperatures, which means the spinel structure has Mn-defects backbone. Mn^{4+} ion remains on the $LiNi_{0.5}Mn_{1.5}O_4$ surface due to its insolubility in the carbonate-based electrolyte. However, Mn^{2+} ion is soluble in the electrolyte and move from the structure of cathode to the graphite surface. The Mn^{2+} ions are reduced on the surface of the graphite material, which results in the capacity fading by Mn deposition and new SEI layer formation at the Mn particle on the graphite`s surface[9,10]. It is difficult to examine the influence of Mn dissolution in the full-cell from the overall capacity fading because the capacity fading comes from Mn dissolution and decomposition of the electrolyte in the traditional cell design simultaneously.

Multi-layer electrolyte cell (MEC) is designed to separate and examine the impact of Mn dissolution from decomposition of the electrolyte shown as figure 1.5[11]. MEC introduces the ceramic solid electrolyte $Li_{1.3}Ti_{1.7}Al_{0.3}(PO_4)_3$ dense pellet to separator the carbonate-base liquid electrolyte into individual positive and negative compartments. The solid electrolyte conduct Li^+ ion selectively, which means that Mn^{2+} ion and other products of the decomposition cannot pass through the solid electrolyte to reach the anode side. Therefore, the capacity fading of graphite/$LiNi_{0.5}Mn_{1.5}O_4$ should be coming from the following sources 1) Li loss by oxidative decomposition of carbonate electrolyte over 4.3V vs. Li/Li^+, 2) Mn loss from spinel structure,

ULSAN NATIONAL INSTITUTE OF SCIENCE AND TECHNOLOGY

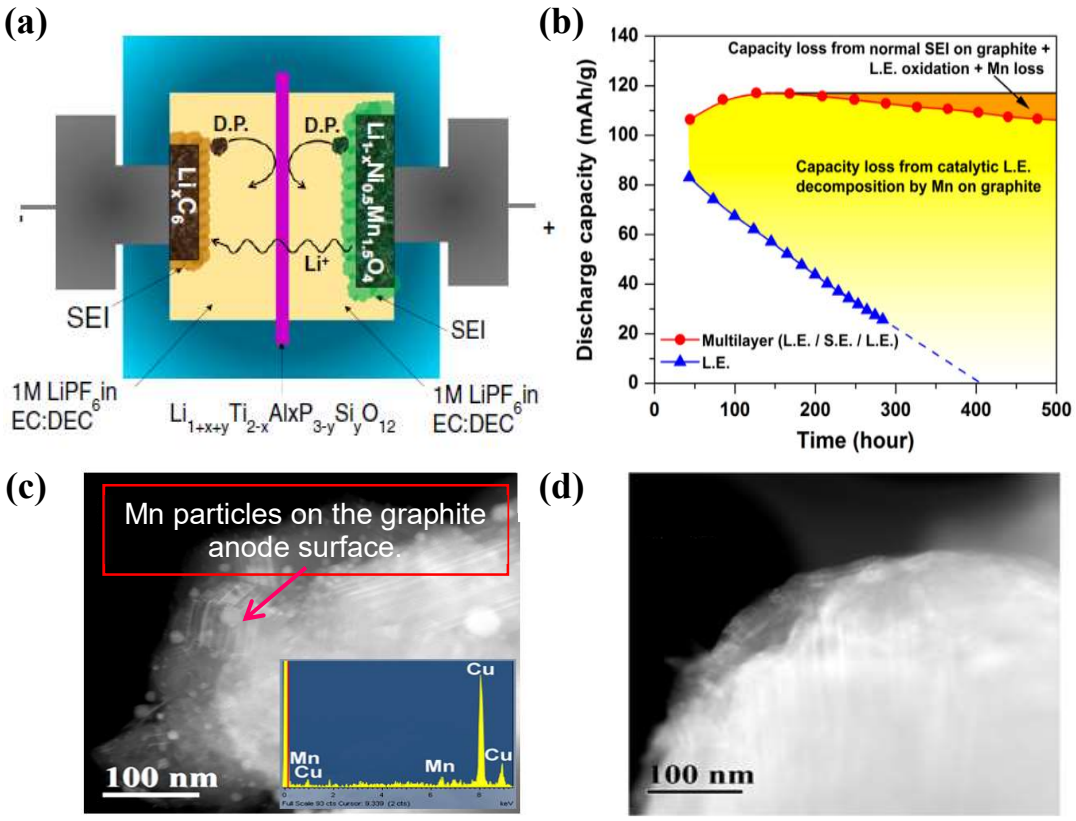

Figure 1.5 (a) Multi-layer electrolyte cell for investigating electrochemical mechanism and impact on high voltage cathode materials, (b) examination of the influence of the Mn dissolution on the LIB full-cell, TEM images of cycled graphite electrode (c) commercial coin cell, (d) MEC [11].

3) Li^+ ion consumption during the general formation of SEI layer on graphite, 4) Li^+ ion consumption by the reduction of Mn^{2+} on graphite ($Mn^{2+} + 2LiC_6 \rightarrow Mn + 2Li^+ +$ graphite), 5) new SEI layer formation at the Mn particle on the graphite. MEC gauges the influence of the Mn dissolution; 4),5) separated from 1), 2), 3). MEC identifies its ability to prevent the crossover of Mn^{2+} ions and to improve the electrochemical performances of the cell. We expect that MEC can test another high voltage materials improving electrochemical reaction of cathode.

This study makes the multi-layer electrolyte cell (MEC) which is composed of three electrolytes: inorganic solid electrolyte, ionic liquid electrolyte, and carbonate-based

ULSAN NATIONAL INSTITUTE OF SCIENCE AND TECHNOLOGY

electrolyte in figure 1.6. Inorganic solid electrolyte separates the ionic liquid electrolyte, carbonate-based electrolyte and side-reaction decomposition product. It also provides the Li ion pathway through them. Ionic liquid electrolytes are reported to have lower HOMO energy level than carbonate-based electrolytes, so they stabilize the electrochemical reaction at high voltage cathode. The carbonate-based electrolyte has stable solid electrolyte interphase layer on anode like Li metal or graphite. Therefore, we will examine the performance of the multi-layer electrolyte cell and improve the properties of the multi-layer electrolyte cell and the high voltage cathode material.

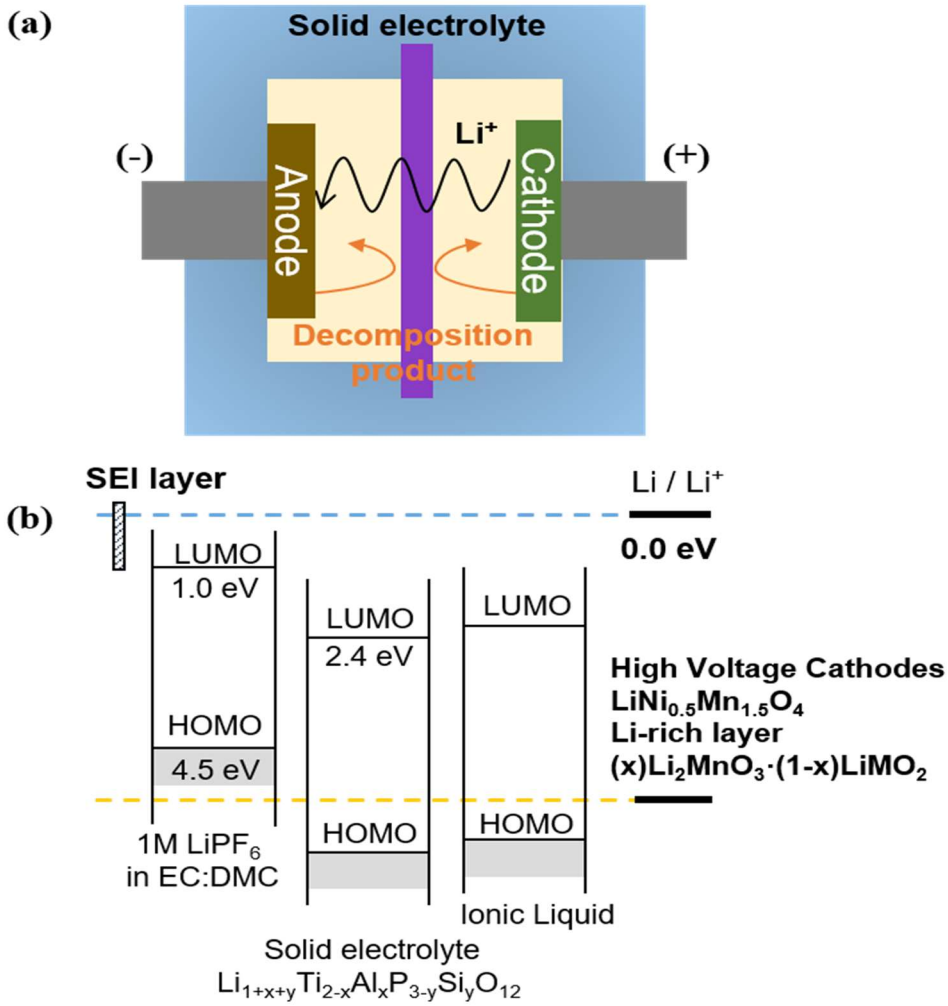

Figure 1.6 (a) Schematic multi-layer electrolyte cell blocking the crossover of the decomposition product, (b) electrochemical potential for the component of the multi-layer electrolyte cell [11].

ULSAN NATIONAL INSTITUTE OF SCIENCE AND TECHNOLOGY

1.3 Lithium ion conducting solid oxide electrolyte

Most inorganic solid electrolyte materials have crystalline structures with a specific framework formed of coordination polyhedral and exhibit anisotropic conductivity to achieve fast ion transport through vacant and interstitial sites in the framework structure[12]. These ion conductors should contain mobile ions with disordered sublattices that are of a suitable size to fit through the smallest cross-sectional area of the conducting channel (termed the bottleneck) in conduction pathways. The optimum concentrations of vacancy and interstitial sites, excess isovalent sites with nearly the same potential energies as those of the occupied sites make stable framework ions with different coordination numbers, and weak interaction forces between the mobile ions and main framework. We classify inorganic solid electrolytes into three types based on the different heteroatoms in their ligand; oxide, sulfide and nitride solid electrolytes. The oxide materials have high moisture stability and wide electrochemical window compared to sulfide and nitride solid electrolyte, so we focus on the oxide materials. We summarize the oxide solid electrolyte in figure 1.7

ULSAN NATIONAL INSTITUTE OF SCIENCE AND TECHNOLOGY

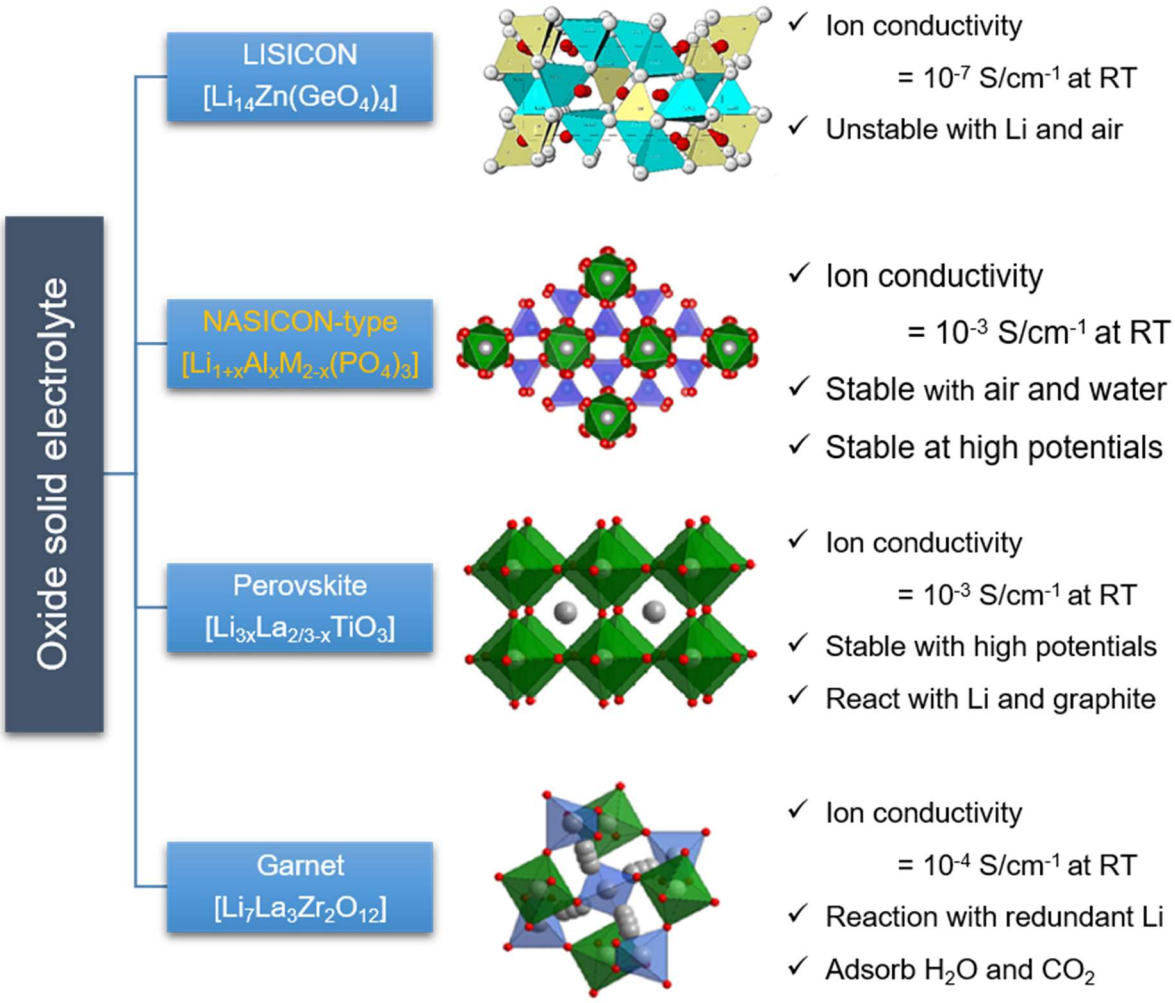

Figure 1.7 Categories of the solid oxide electrolyte

ULSAN NATIONAL INSTITUTE OF SCIENCE AND TECHNOLOGY

1.3.1 Lithium superionic conductors

As early as 1978, Hong reported $Li_{14}Zn(GeO_4)_4$ with a conductivity of 0.13 S cm^{-1} at 300 ℃. $Li_{14}Zn(GeO_4)_4$ can be a solid solution of Li_4GeO_4 and Zn_2GeO_4 with a three-dimensional $[Li_{11}Zn(GeO_4)_4]_3$- anion skeleton. The additional lithium ion in this Li-rich solution based on γ-Li_2ZnGeO_4 occupies interstitial octahedral sites[13] and the extremely elevated temperature factors of the remaining three lithium ion render them more mobile. At the same time, every O^{2-} forms strong covalent bonds with the skeleton cations so that the oxygen charge density is polarized away from Li^+ and the interaction force with the mobile Li^+ weakens, giving rise to a low migration activation energy of about 0.24eV. LISICON-type electrolytes can operate at elevated temperatures because of their thermal stability and near-zero vapor pressure as well as their stability in the presence of water and aqueous electrodes. Even so, most LISICON electrolytes have been reported to have low ionic conductivity at room temperature (10^{-7} S cm^{-1}), and they suffer from instability with Li and air[14,15,16].

1.3.2 Sodium superionic conductors

Sodium superionic conductor (NASICON) $Na_{1+x}Zr_2P_{3-x}Si_xO_{12}$ was reported by Goodenough et al in 1976 [17]. The crystalline NASICON framework substitutes partial P with Si in $NaM_2(PO_4)_3$ and consists of corner-sharing PO_4 tetrahedron and MO_6 octahedron assembled to form a 3D network structure[17]. This material maintains its original NASICON structure and turns into a lithium conductor when the sodium ions are replaced by lithium ions. This lithium conductor has lower ionic conductivity than that of the sodium conductor. The original channels suitable for Na^+ are too large for Li^+ because of Li^+ has a smaller ionic radius than Na^+. Li-O bonds are more covalent and stronger than Na-O bonds, Li^+ is less mobile than Na^+. The partial substitution of framework ions with different elements is studied to optimize the

ULSAN NATIONAL INSTITUTE OF SCIENCE AND TECHNOLOGY

performance, especially the ionic conductivity. Because trivalent Al has a smaller ionic radius (0.53Å) than those of Ti and Ge, the partial substitution Ti with Al in $LiTi_2(PO_4)_3$ and Ge in $LiGe_2(PO_4)_3$ results in $Li_{1+x}Ti_{2-x}Al_x(PO_4)_3$ (LTAP) and $Li_{1+x}Ge_{2-x}Al_x(PO_4)_3$ (LGAP) respectively, which possess higher ionic conductivity than before[18]. The reason why these Al-doped electrolytes displayed remarkable enhancement of conductivity was that favorable conductive phases of LTAP and LGAP with a small uniform grain boundary are generated[18]. The highest conductivities at room temperature of LTAP and LGAP are 10^{-3} and 10^{-2} S cm^{-1} respectively. Because they have different space-charge effects, the grain-boundary resistances of LGAP were lower than those of LTAP[19,20]. NASICON-type electrolytes have the advantages of their high ionic conductivity, high moisture stability and wide electrochemical window of about 7V. However, the typical shortcoming of LTAP materials is the reduction of Ti^{4+} by the metallic Li anode. Therefore, the Ti-free NASICON compound LGAP is the candidate for application in the future.

1.3.3 Perovskites

A perovskite structure ABO_3 ($Li_{3x}La_{2/3-x}TiO_3$) displays a high bulk conductivity of 10^{-3} S cm^{-1} at room temperature[21]. Univalent Li and trivalent La occupy the A-sites in the perovskite-type framework supported by corner-sharing TiO_6 octahedral. The presence of La with its larger radius and higher valence results in more numerous vacancies, allowing Li^+ to migrate efficiently through the defect-type mechanism to attain high bulk-ionic conductivity[22,23]. The bottleneck is surrounded by two A-sites and four O ions, and its size is the predominant factor controlling the activation energy for ionic conductivity[24]. Despite its high conductivity at room temperature, the application of (Li, La)TiO_3 as a solid electrolyte is not favorable because the compound rapidly reacts with lithium anode leading to the reduction of Ti^{4+} to Ti^{3+} [25].

ULSAN NATIONAL INSTITUTE OF SCIENCE AND TECHNOLOGY

1.3.4 Garnet

A general garnet has chemical formula of $A_3B_2(XO_4)_3$ (A=Ca, Mg, Y, La or rare earth; B=Al, Ga, Ge, Mn, Ni or V; X=Si, Ge, Al) where A, B and X are cation sites with eight, six and four coordinated O ions, respectively[26]. Thangadurai and Weppner reported novel garnet-type conductors, nominal chemical compositions $Li_5La_3M_2O_{12}$ (M=Nb or Ta) and $Li_6Al_2M_2O_{12}$ (A=Ca, Sr or Ba; M=Nb or Ta)[27]. After that, they announced a promising zirconium-containing garnet-like conductor, $Li_7La_3Zr_2O_{12}$ with total conductivity of 3 x 10^{-4} S cm^{-1} [28]. These garnet-type compounds show exceptional electrochemical stability of about 6V vs. Li metal and low electronic conductivity[29]. It is also noteworthy that the inter- and intra-grain conductivities of these materials are the same order of magnitude[30]. However, these garnet-type compounds are limited by their reactivity with redundant lithium and adsorbed H_2O or CO_2.

Overall, most oxide solid electrolytes exhibit low ionic conductivities and reactivity to moisture and air, but some oxide materials such as NASICON-type, perovskite possess high ionic conductivities enough to apply and have stability to moisture and air. Therefore, we use the NASICON-type solid electrolyte for multi-layer electrolyte because NASICON-type structure can avoid the reaction to lithium metal.

ULSAN NATIONAL INSTITUTE OF SCIENCE AND TECHNOLOGY

1.4 Ionic liquid electrolyte

A species of salt that has a low melting point below room temperature is generally called room temperature ionic liquid (RTIL). These ionic liquids have been studied as lithium-ion electrolyte. RTIL usually have a molecular ionic salt such as quaternary ammonium $[R_4N]^+$ or based on cyclic amines, both aromatic (pyridinium, imidazolium) and saturated (piperidinium, pyrrolidinium), shown as figure 1.8. Cations could be extended by incorporating functional group of the cyclic structures. As well, anions may be based on structure of inorganic halide and cyano groups, such as $[Ag(CN)_2]^-$, $[C(CN)_3]^-$, or $[N(CN)_2]^-$. There are many combinations of cation and anion, which determine the ionic liquid physical, electrochemical properties; conductivity, electrochemical stability. Some of the most popular RTILs as electrolyte for LIB are N-butyl-N-methylpyrrolidinium bis(triflruoromethanesulfonyl)imide (Py_{14} TFSI) and 1-Ethyl-3-methylimidazolium bis(trifluoromethylisulfonyl)imide (EMI TFSI). Their ion conductivities are determined by molar concentration (c_i) and viscosity (η) according to stokes law $\sigma = ((z_i)^2 F c_i) / (6\pi\eta r_i)$ [31]. These ionic liquids are reported to have ionic conductivities of 10^{-3} S cm^{-1} at room temperature comparable to carbonate-based electrolytes and wide electrochemical windows (>5 V vs. Li/Li^+)[32]. Their application in LIB has been widely studied and reported[33–40]. In this study, ionic liquid electrolytes are used to repress the oxidation decomposition of the electrolyte at high potential. Their good electrochemical stability for oxidative reactions, thermal stability and non-flammability compared to the carbonate-base electrolyte currently commercialized in LIB, may result in improved stability performance at high potential cathode and elevated temperatures, which could match the x $Li_2MnO_3 \cdot$ (1-x) $LiMO_2$ cathode materials [34,35,41].

ULSAN NATIONAL INSTITUTE OF SCIENCE AND TECHNOLOGY

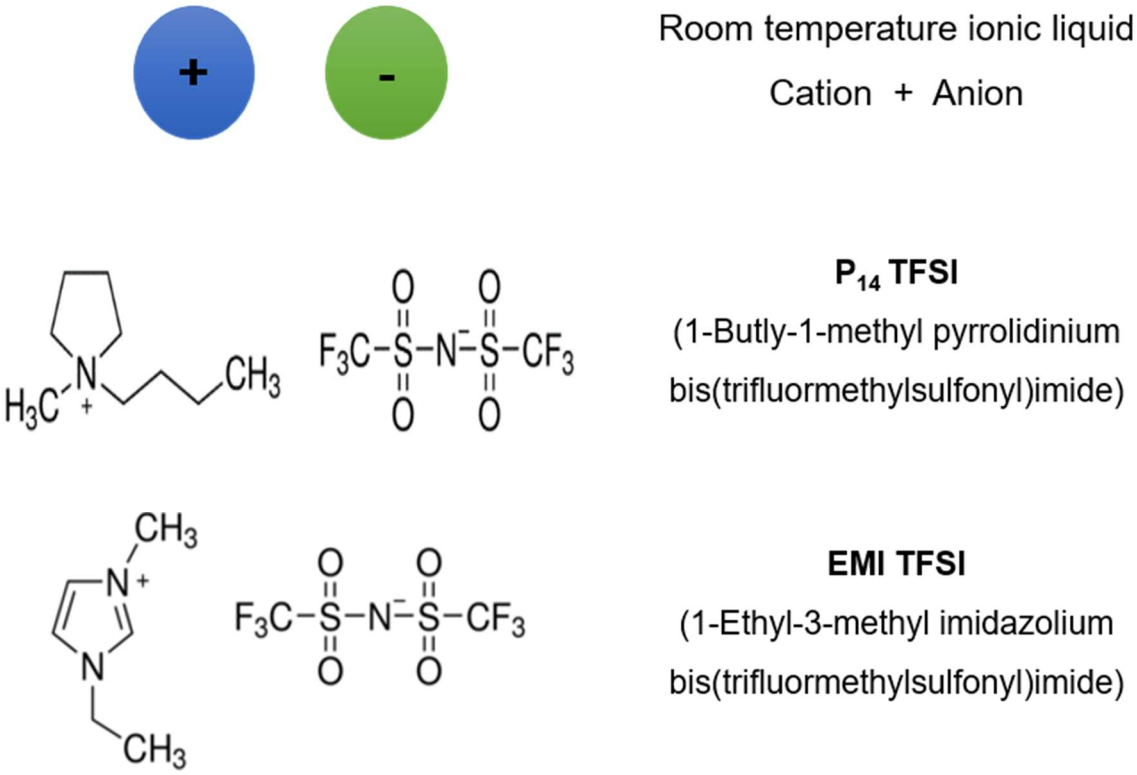

Figure 1.8 Structure of ionic liquids

ULSAN NATIONAL INSTITUTE OF SCIENCE AND TECHNOLOGY

1.5 Over-lithiated layered oxide (OLO) cathode materials

Over-lithiated layered oxide x Li_2MnO_3 · (1-x) $LiMO_2$ materials have been reported to be promising candidates for high energy density. OLO materials have high capacity, over 200 $mAhg^{-1}$, and high operating potential up to ~4.8 V vs. Li/Li^+. These OLOs have been notated with two completely different structural understanding: composite two component x Li_2MnO_3 · (1-x) $LiMO_2$ (M = Mn, Ni, Co, Fe, Cr, etc.) and solid-solution $Li_{1+(x/(2+x))}Mn_{2x/(2+x)}M_{(2-2x)/(2+x)}O_2$ (M = Mn, Ni, Co, Fe, Cr, etc.)[42,43]. Both notations are equal to the same materials. To grasp the complicated electrochemical reaction mechanism during first and following galvanostatic cycles of these OLO materials, a three-dimensional compositional phase diagram is shown in figure 1.9. The $LiMO_2$ components are charged up to 4.4V and Li_2MnO_3 components are activated over 4.5V vs. Li/Li^+. The Li_2MnO_3 component with tetravalent manganese cation and monovalent lithium cation is difficult for tetravalent manganese cation to oxidize during charging. Instead of the oxidation of tetravalent manganese cation, the divalent oxygen anion is oxidized and oxygen gas is released shown as the reaction equations below.

$$LiMO_2 \rightarrow Li^+ + e^- + MO_2 \text{ (under 4.5V)}$$

$$Li_2MnO_3 \rightarrow 2Li^+ + 2e^- + MnO_2 + 1/2O_2\uparrow \text{ (over 4.5V)}$$

The reaction of the Li_2MnO_3 components is irreversible because oxygen gases are released from the Li_2MnO_3 components and their phase composition changed. However, it is difficult to examine whether and how much the new phase in MnO_2 changes exactly. During the first galvanostatic discharge process, Li^+ ions insert into the MO_2 phase and newly formed MnO_2 components, while the inactivated Li_2MnO_3 structure remain in these complex layered materials[44–46]. Therefore, the electrochemical reaction trace and composition state should be in the intermediate chemical composition Li_2MnO_3, $LiMnO_2$, and $LiMO_2$.

ULSAN NATIONAL INSTITUTE OF SCIENCE AND TECHNOLOGY

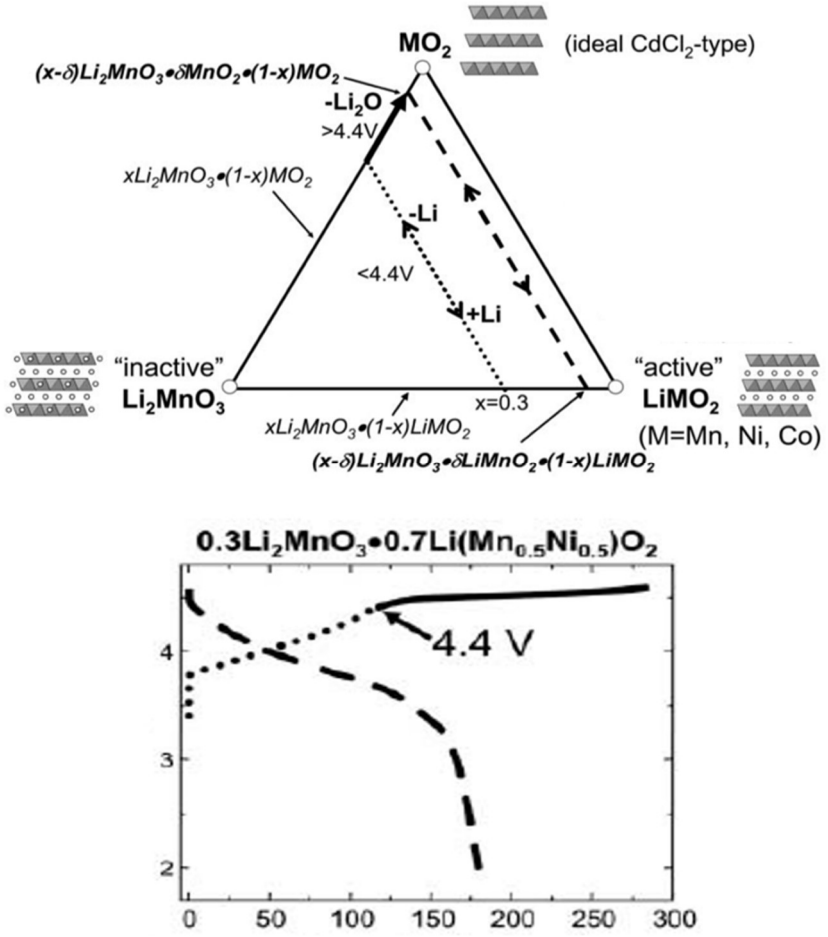

Figure 1.9 Compositional phase change during the electrochemical reaction pathway for x Li_2MnO_3·(1-x) $LiMO_2$ materials [42].

The operating temperature and the current density during the cycle are considered crucial factors to influence the Li_2MnO_3 activation and reversible capacity. As seen in Fig. 1.10, two respective cells were cycled at different temperatures. The low C-rate and elevated temperature raised the charge and discharge capacity of Li / $Li_{1.2}Ni_{0.15}Mn_{0.55}Co_{0.1}O_2$ half-cell. The harsh conditions of a high temperature and high voltage accelerate the possible electrochemical redox reaction of cations in a solid matrix (Mn^{4+}/Mn^{5+}, Mn^{5+}/Mn^{6+}) and redox reaction of anion on surface (O^{2-}/O_2^{2-}) in terms of lithium insertion scheme[46 47]. Naoaki et al reported that OLOs represent extra discharge capacity from electrochemical OLO`s surface reaction of the oxygen

ULSAN NATIONAL INSTITUTE OF SCIENCE AND TECHNOLOGY

molecules[46]. During the first charge, Li_2MnO_3 component changes into MnO_2, oxygen molecules occur at 4.5V vs. Li/Li^+ plateau. The oxygen molecules existinged inside the cell are electrochemically reduced in the subsequent discharge below 3.0V, leading to the extra capacity. The reaction mechanism of these OLOs at elevated temperatures may be different and more complicated compared with those at room temperature.

The oxidative decomposition of electrolyte and electrochemical reaction mechanism of cathode materials occur at the interface between cathode and electrolyte. Since the condition with 4.3 V vs. Li/Li^+ negatively affects the reversibility of the phase on cathode material and interface between cathode and electrolyte, it is difficult to comprehend the mechanism and reaction on the cathode. The oxygen released from Li_2MnO_3 component could react with cathode`s surface mysteriously or cross over into anode, affecting the performance of the OLO materials through an unknown mechanism. Therefore, the Multi-layer electrolyte cell (MEC) separates the electrolyte into two compartments, so preventing the crossover of the oxygen released from Li_2MnO_3 component to anode side like Mn dissolution as shown in figure 1.5. MEC could replace carbonate-based electrolyte for cathode side with ionic liquid electrolyte which is reported to have good electrochemical stability for oxidative reaction, thermal stability and non-flammability compared to the carbonate-bases electrolyte currently commercialized in LIB. The organic carbonates are used by the anode`s side electrolytes that are stable for lithium metal or graphite.

ULSAN NATIONAL INSTITUTE OF
SCIENCE AND TECHNOLOGY

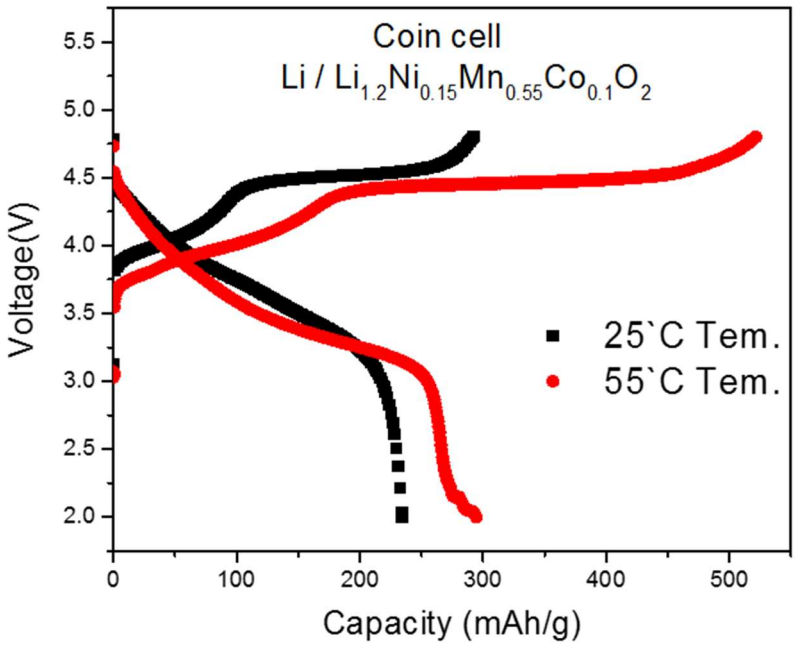

Figure 1.10 Voltage profile of first cycle half-cell for Li / $Li_{1.2}Ni_{0.15}Mn_{0.55}Co_{0.1}O_2$ at C/10 rate and different temperature

ULSAN NATIONAL INSTITUTE OF SCIENCE AND TECHNOLOGY

1.6 Experiment

1.6.1 Preparation of ionic liquid electrolyte and electrode

Ion liquids 1-ethyl-3-methylimidazolium bis (trifluoromethylsulfonyl) imide (EMI TFSI), 1-butyl-1-methyl pyrrolidinium bis (trifluoromethylisulfonyl) imide (Py_{14} TFSI) and lithium bis (trifluoromethylisulfonyl) imide (Li salt) were purchased from sigma-aldrich. The lithium salt, Py_{14} TFSI (1: 9 mol ratio) and EMI TFSI (1: 9 mol ratio) ionic liquid electrolyte were made respectively. The electrochemical stability window of ionic liquid was measured using Li metal as counter electrode and reference electrode, Voltammetry (LSV) was measured carbonate-based liquid electrolyte 1.0M $LiPF_6$ in ethylene carbonate: dimethyl carbonate (1: 1 vol%) that was purchased from Panax Etec.

The cathode material $Li_{1.2}Ni_{0.15}Mn_{0.55}Co_{0.1}O_2$ material, different notation $0.4Li_2MnO_3 \cdot 0.4LiNi_{0.375}Mn_{0.375}Co_{0.25}O_2$, was obtained from the Argonne national laboratory. A positive electrode slurry was prepared by mixing 80 wt% $Li_{1.2}Ni_{0.15}Mn_{0.55}Co_{0.1}O_2$, super P 10 wt%, and pvdF 10 wt% dissolved in NMP solvent (N-methyl-2-pyrrolidinon). The slurry was cast onto aluminum foil at a density of 2.5 mg/cm^2. The prepared cathode was dried in an 80 ° C oven for 2 hours and rolled to press electrode. The dried electrode was stored in a vacuum oven at 80 ° C for one day.

1.6.2 Synthesis of inorganic electrolyte

Preparation of the $Li_{1.3}Ti_{1.7}Al_{0.3}(PO_4)_3$ was made with process[11,20,48,49,47–51]. LiCl, $Al(NO_3)_3 \cdot 9H_2O$, $NH_4H_2PO_4$ were dissolved in distilled water according to the stoichiometry. Added $Ti(OC_4H_9)_4$ to the homogeneously dissolved solution. Continuous ball-milled the precursor solution for 24h. Spray – dryed the precursor solution to obtain uniform shape of

ULSAN NATIONAL INSTITUTE OF SCIENCE AND TECHNOLOGY

precursor powder. $Li_{1.3}Ti_{1.7}Al_{0.3}(PO_4)_3$ powder was obtained through primary heat treatment 400 °C 2h and secondary heat treatment 900 °C 4h.

To make LTAP pellets, LTAP powder was pelletized at a pressure of 40 MPa in a first-round mold, then molded at 200 MPa by secondary cold isostatic press method. Molded pellets were heat treated at 900 ° C for 10h to form LTAP pellets.

To make a porous LTAP pellet, we mixed the LTAP powder and the precursor components at a certain ratio to make an aqueous solution and obtain a homogeneous powder with a spray - dryer. A homogeneous mixture is made into a pellet at a pressure of 40 MPa in a primary round mold, and then molded into a 200 MPa by cold isostatic press method. Heat the formed pellet to 900 ° C 10h. Syntheses the precursor with LTAP and leaves pores as the gaseous components fly. Porosity was analyzed by thermogravimetric analysis and theoretical density. In order to measure the ionic conductivity of OHARA product, it was measured by AC impedance after Pt coating.

1.6.3 Assembly of the multi-layer electrolyte cell

Figure 1.6 shows the conceptual diagram of the Multi-layer electrolyte cell (MEC) and electrochemical potential for the MEC components. MEC uses ionic liquid electrolyte, carbonate-based electrolyte, electrode, current collector (Cu, Ni, Al). Dense ceramic $Li_{1.3}Ti_{1.7}Al_{0.3}(PO_4)_3$ pellet was purchased from OHARA. The thickness of pellet was 0.8 mm and it was sealed in the form of pouch completely separating the electrolyte of the anode and the electrolyte of the cathode. The carbonate electrolytes 1.0M $LiPF_6$ in EC: DMC (1: 1 vol%) and ionic liquid electrolyte LiTFSI 0.1 mol% in Py_{14} TFSI, LiTFSI 0.1 mol% in EMI TFSI were used. The cathode composition was composed of 80 wt% of $Li_{1.2}Ni_{0.15}Mn_{0.55}Co_{0.1}O_2$, 10

ULSAN NATIONAL INSTITUTE OF SCIENCE AND TECHNOLOGY

wt% of super P, 10 wt% of PvdF, and maintained a loading density of 2.8 mg / cm^2 in an aluminum current collector by making slurry uniformly with a think mixer. It is used by bonding to lithium metal anode and Nickel current collector.

1.6.4 Assembly of the porous pellet-type multi-layer electrolyte cell

Porous pellet type cells were made using Swagelok cells. The fabricated porous LTAP pellet was impregnated with an ionic liquid Py_{14} TFSI. After a small amount of ionic liquid was pelletized and the cathode was left in a vacuum for a certain period, the ionic liquid was inserted between the porous of the pellet. A 1.0 M $LiPF_6$ in EC: DMC (1: 1 vol%) with a glass fiber separator between the pellet and Li metal was used.

ULSAN NATIONAL INSTITUTE OF SCIENCE AND TECHNOLOGY

1.7 Result and Discussion

The ceramic solid electrolyte $Li_{1.3}Ti_{1.7}Al_{0.3}(PO_4)_3$ pellet was introduced into Multi-layer electrolyte cell to separate electrolytes into cathode and anode compartment. To measure the ion conductivity of the OHARA pellet $Li_{1.3}Ti_{1.7}Al_{0.3}(PO_4)_3$, the pellet was plated with Pt to measure the AC impedance. The electrical conductivity of the NASICON-tpye structure is very low, so the electrical conductivity was negligible considering the influence of ionic conductivity and electrical conductivity of electrochemical impedance spectroscopy as shown in figure 1.11. The ion conductivity of the pellet was calculated as Ion conductivity = d / R x A, where d = distance between two electrodes, R = electrolyte resistance, and A = electrode Area. The ionic conductivity of the OHARA pellet was measured as 1.9 x 10^{-4} S/cm.

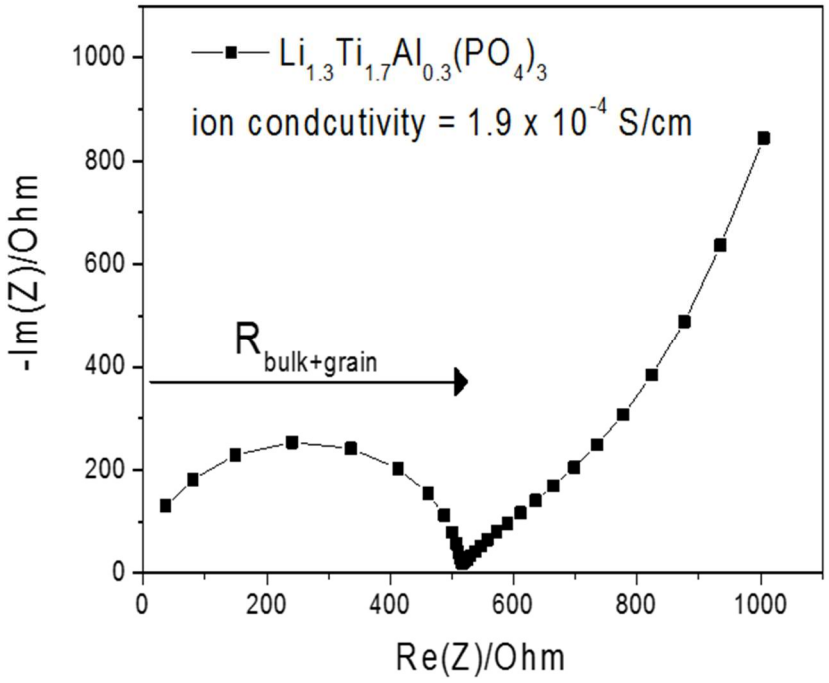

Figure 1.11 Electrochemical impedance spectroscopy of ceramic electrolyte $Li_{1.3}Ti_{1.7}Al_{0.3}(PO_4)_3$ pellet.

ULSAN NATIONAL INSTITUTE OF SCIENCE AND TECHNOLOGY

Oxidation stability of some of liquid electrolytes was measured by linear sweep voltammetry. Lithium metal anode was employed as a counter electrode and reference electrode to measure the oxidative decomposition current of liquid electrolytes generated at the working electrode. As seen in figure 1.12 (a), commercial carbonate liquid electrolyte 1.0M $LiPF_6$ in EC: DMC (1: 1) showed the oxidation decomposition current peak at 4.3V vs. Li/Li^+. Ionic liquid electrolyte LiTFSI 0.1 mol% in EMI TFSI electrolyte showed small oxidation peak 4.6V vs. Li/Li^+ and main electrolytic decomposition reaction of EMI TFSI occured at over 5.1V.

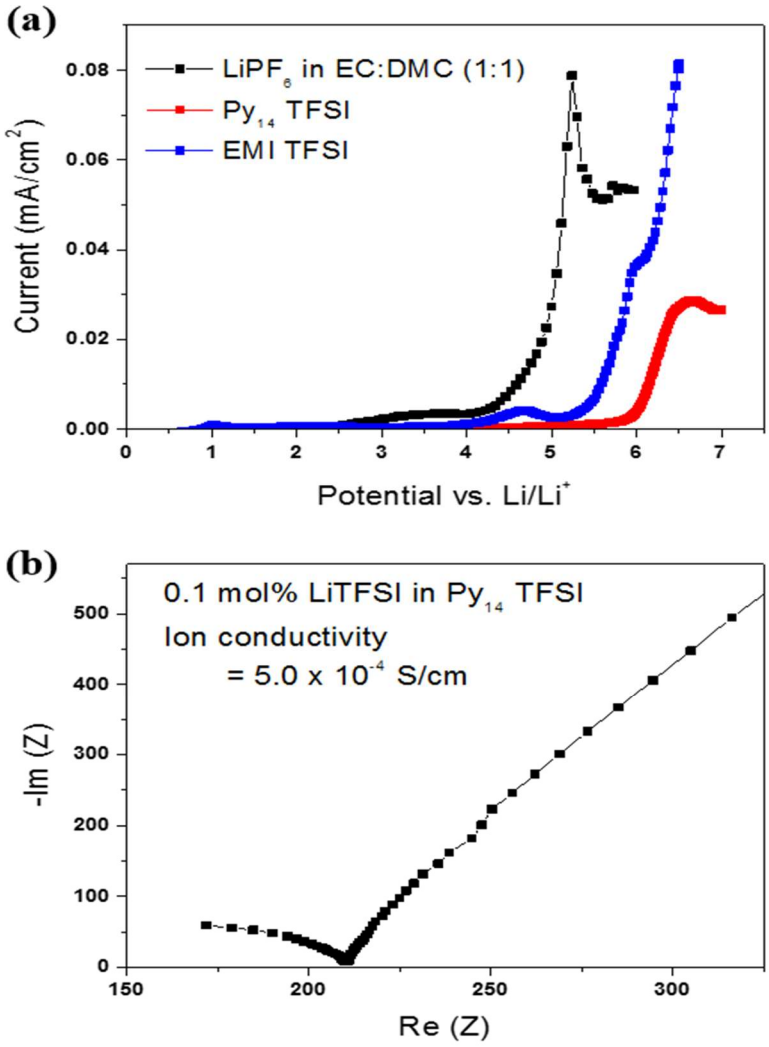

Figure 1.12 (a) Linear sweep voltammetry for the ionic liquid electrolytes, (b) ion-conductivity of the 1-Butyl-1-methyl pyrrolidinium bis(trifluoromethylsulfonyl)imide.

ULSAN NATIONAL INSTITUTE OF SCIENCE AND TECHNOLOGY

LiTFSI 0.1 mol% in Py_{14} TFSI electrolyte has a higher voltage stability than LiTFSI 0.1 mol% in EMI TFSI. Therefore, Py_{14} TFSI ionic liquid electrolyte was applied to cathode-side electrolyte of multi-layer electrolyte cell. The ion conductivity of the Py_{14} TFSI measured 5.0 x 10^{-4} S/cm by electrochemical impedance spectroscopy as shown in figure 1.12 (b). Ionic liquid electrolyte had lower ion conductivity than carbonate-based electrolyte and high viscosity, which caused theionic liquid electrolyte not tohave good interface with ceramic solid electrolyte $Li_{1.3}Ti_{1.7}Al_{0.3}(PO_4)_3$ pellet. We will improve the limitation of multi-layer electrolyte cell by expansion of the contact area with solid electrolyte and ionic liquid electrolyte.

The over-lithiated layerd oxide material has a high capacity of more than 200 mAh / g and is attracting attention as a next generation LIB cathode material. In particular, it is believed that this material has a higher capacity (over 300 mAh / g) at higher temperatures and a reaction mechanism that is different from room temperature. We tested at 55 ° C to maximize the

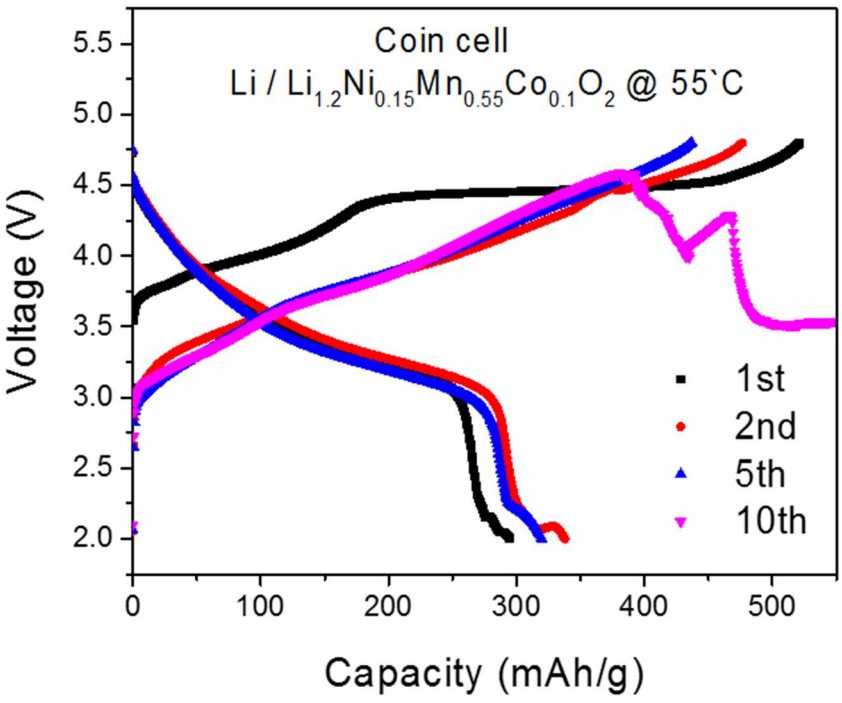

Figure 1.13 Charge and discharge voltage profile for Li / $Li_{1.2}Ni_{0.15}Mn_{0.55}Co_{0.1}O_2$ half-cell at C/10 rate and 55`C.

ULSAN NATIONAL INSTITUTE OF SCIENCE AND TECHNOLOGY

stability impact of multi-layer electrolyte cells. As seen in figure 1.13, Li / $Li_{1.2}Ni_{0.15}Mn_{0.55}Co_{0.1}O_2$ half-cell test using coin cell conventional electrolyte showed high capacity close to 300 mAh/g at 1/10 C-rate (1C = 377 mAh/g). However, it had low coulombic efficiency and cell death after 10 cycles due to thermal stability problem. As seen in figure 1.14, Multi-layer electrolyte cell (MEC) of (1.0M $LiPF_6$ in EC: DMC (1:1) / Solid electrolyte / 1.0M $LiPF_6$ in EC: DMC (1:1)) has higher thermal stability compared to that of coin cell. Although conventional liquid electrolytes are oxidized over 4.3V potential and 55`C harsh conditions, MEC has reasonable capacity up to 15 cycle number. We expect to improve stability by replacing conventional liquid electrolytes with ionic liquid.

ULSAN NATIONAL INSTITUTE OF SCIENCE AND TECHNOLOGY

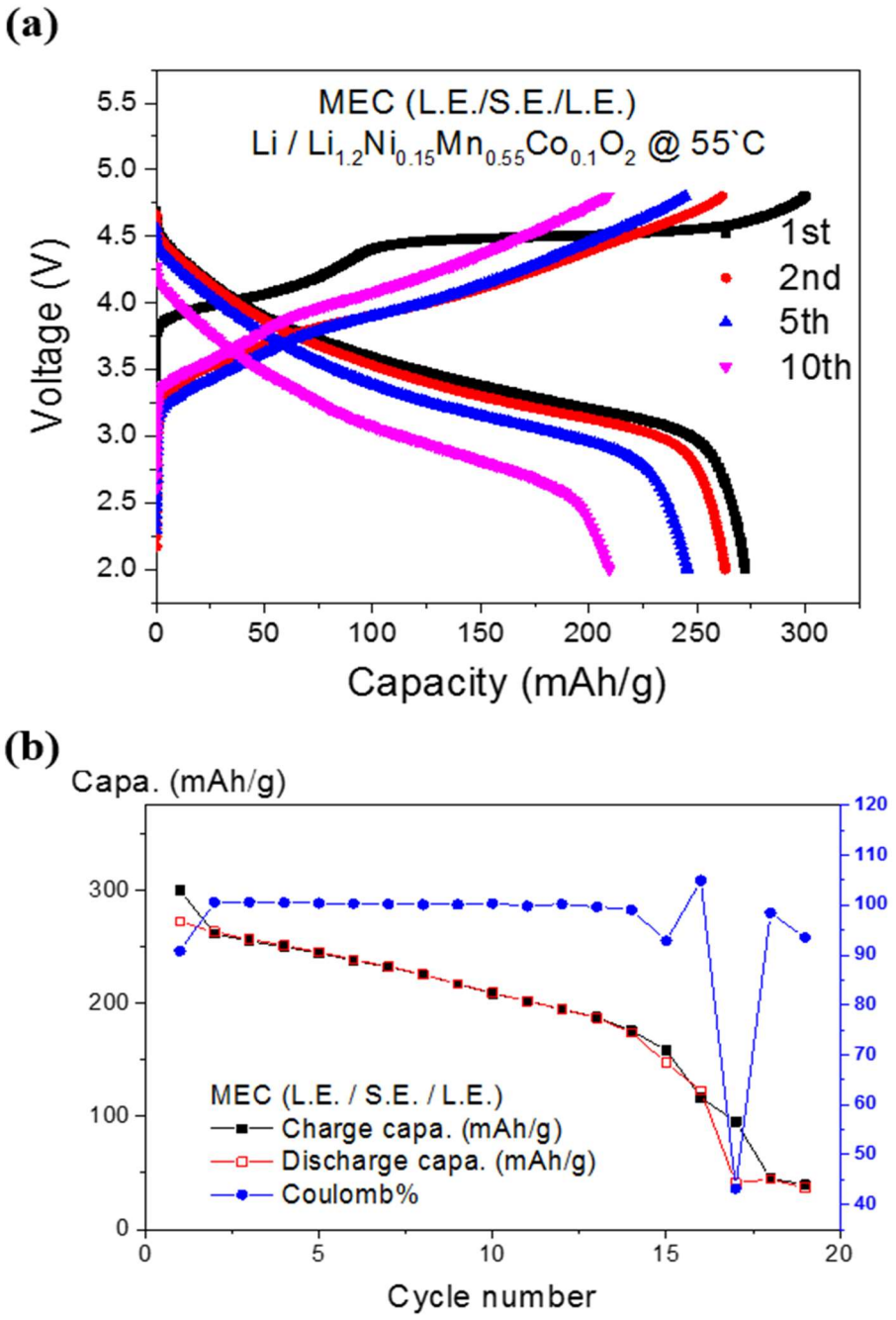

Figure 1.14 (a) Charge and discharge voltage profile showing voltage vs. capacities (b) capacity vs. cycle number for Multi-layer electrolyte cell (1.0M $LiPF_6$ in EC: DMC (1:1) / Solid electrolyte / 1.0M $LiPF_6$ in EC: DMC (1:1)) of Li / $Li_{1.2}Ni_{0.15}Mn_{0.55}Co_{0.1}O_2$ at C/10 rate and 55`C.

ULSAN NATIONAL INSTITUTE OF SCIENCE AND TECHNOLOGY

As seen in figure 1.15 (a), Multi-layer electrolyte cell using ionic liquid (1.0M $LiPF_6$ in EC: DMC (1:1) / Solid electrolyte / 0.1 mol% LiTFSI in Py_{14} TFSI) has reversible capacity during cycle. It is suspected that the oxidation of conventional carbonate-base liquid electrolyte over high voltage (4.3V) aggravates the structural changes of the cathode materials compared to figure 1.13 and 1.14 (a). Multi-layer electrolyte cell (1.0M $LiPF_6$ in EC: DMC (1:1) / Solid electrolyte / 0.1 mol% LiTFSI in Py_{14} TFSI) delivers less 200 mAh/g discharge capacity at 1/30 C-rate 55`C while conventional coin cell exhibits approximately 300 mAh/g at 1/10 C-rate 55`C. It is caused by the polarization losses and internal impedance in the cell associated with the electrochemical reactions. The polarization losses include activation polarization and concentration polarization. The activation polarization is caused by overcoming the energy barrier (activation energy) for Li^+ ion in LIB of the slowest reaction among the reaction mechanism which determines the rate of the overall reaction. Overcoming the energy barrier results in a shift in the potential of the cell. The concentration polarization is caused by the concentration difference of species near the surface of the electrode and in the bulk electrolyte when the rate determining step is the mass transfer of a specie among reactants.

The other significant loss which affects the performance and operating potential is internal resistance of the cell which is usually referred to as Ohmic polarization. The Ohmic polarization is caused by the ionic conductivity of the electrolyte, electronic resistance of the active materials and current collectors and the interfacial resistance between them. All internal resistances are defined as $R_{internal}$. To maintain Ohm`s law, which is the linear relationship between potential and current, the potential of the cell will drop to preserve the load current. The operating voltage of a cell connected to an external load R can be expressed as;

$$E = E^\circ - [(\eta_{ct})_{anode} + (\eta_c)_{anode} + (\eta_{ct})_{cathode} + (\eta_c)_{cathode}] - iR_{internal} = iR_{external}$$

ULSAN NATIONAL INSTITUTE OF SCIENCE AND TECHNOLOGY

where E° is the open circuit of the cell, the activation polarization of cathode and anode are designated by the $(\eta_{ct})_{anode}$, $(\eta_{ct})_{cathode}$, respectively. The concentration polarization for anode and cathode are represented by the $(\eta_c)_{anode}$, $(\eta_c)_{cathode}$ respectively. The letter "i" is the operating current on load. If a cell operates at a high current, the operating voltage will widen the gap to the open circuit voltage(OCV). Figure 1.15 (b) shows the polarization losses including

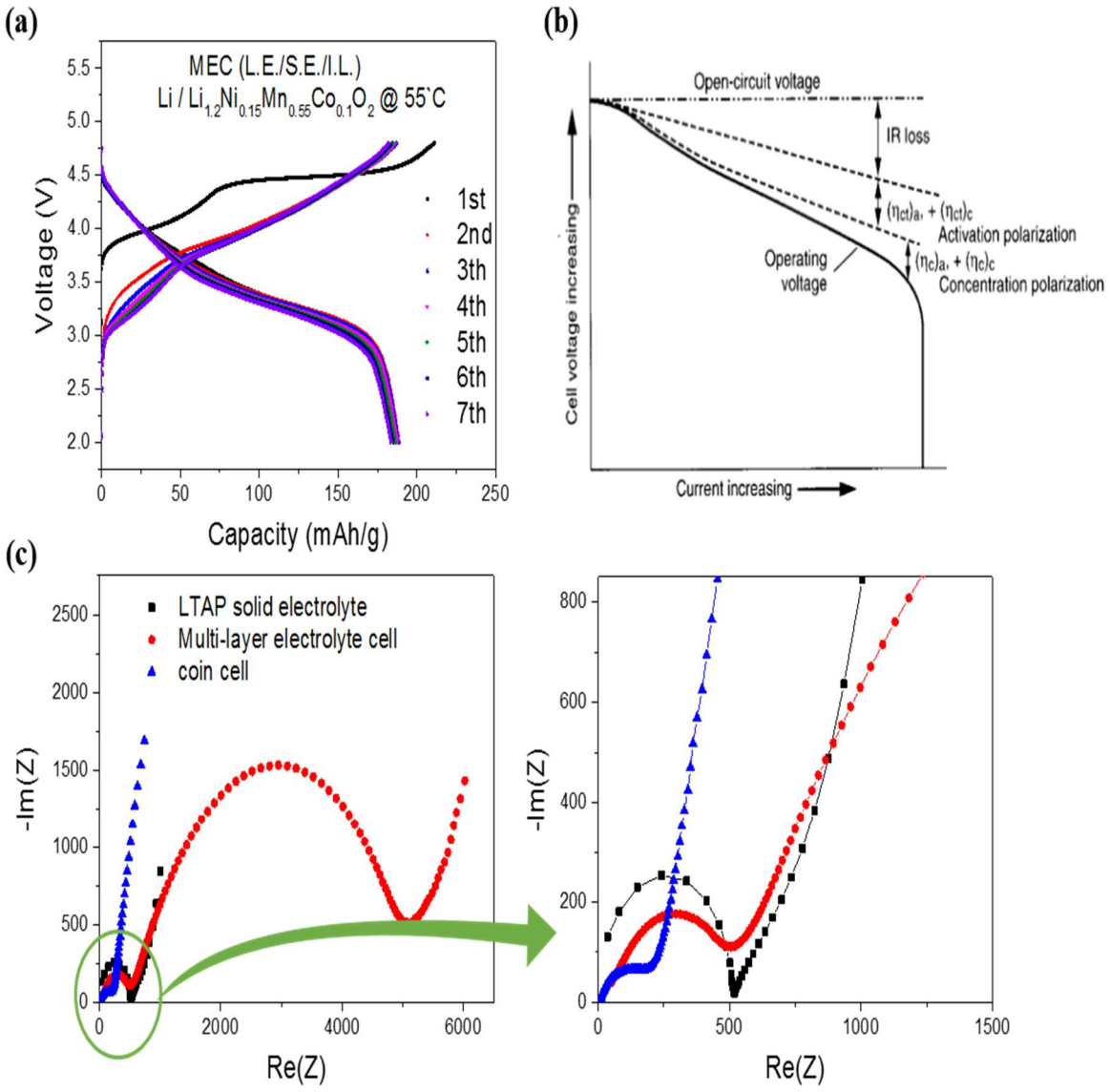

Figure 1.15 (a) Charge and discharge voltage profile for Multi-layer electrolyte cell (1.0M $LiPF_6$ in EC:DMC (1:1vol/vol%) / S.E. / 0.1mol% LiTFSI in $Py_{14}TFSI$) of Li / $Li_{1.2}Ni_{0.15}Mn_{0.55}Co_{0.1}O_2$ at C/30 rate and 55`C (b) polarization effectors on voltage variations (c) electrochemical impedance spectroscopy for multi-layer electrolyte cell of Li / $Li_{1.2}Ni_{0.15}Mn_{0.55}Co_{0.1}O_2$.

ULSAN NATIONAL INSTITUTE OF SCIENCE AND TECHNOLOGY

activations, concentrations, internal resistances of a cell as functions of operating current. Although low current (1/30C-rate) is loaded at the multi-layer electrolyte cell, as shown in figure 1.15 (a), MEC has high polarization and less capacity compared to coin cell. Figure 1.15 (c) shows that MEC has much higher resistance than that of coin cell and there are two semi-circles. First small semi-circle is regarded as one for solid electrolyte $Li_{1.3}Ti_{1.7}Al_{0.3}(PO_4)_3$ used in multi-layer electrolyte cell. The other big semi-circle is due to ionic liquid defined in cathode compartment, which should have high resistance with solid electrolyte and interface resistance with cathode`s surfaces.

Figure 1.16 shows that MEC (1.0M $LiPF_6$ in EC: DMC (1:1) / Solid electrolyte / 0.1 mol% LiTFSI in Py_{14} TFSI) without active materials has second semi-circle resistance through electrochemical impedance spectroscopy. It is the interface resistance between ceramic electrolyte and ionic liquid. This interface resistance makes it difficult to transfer Li^+ ion charge between them.

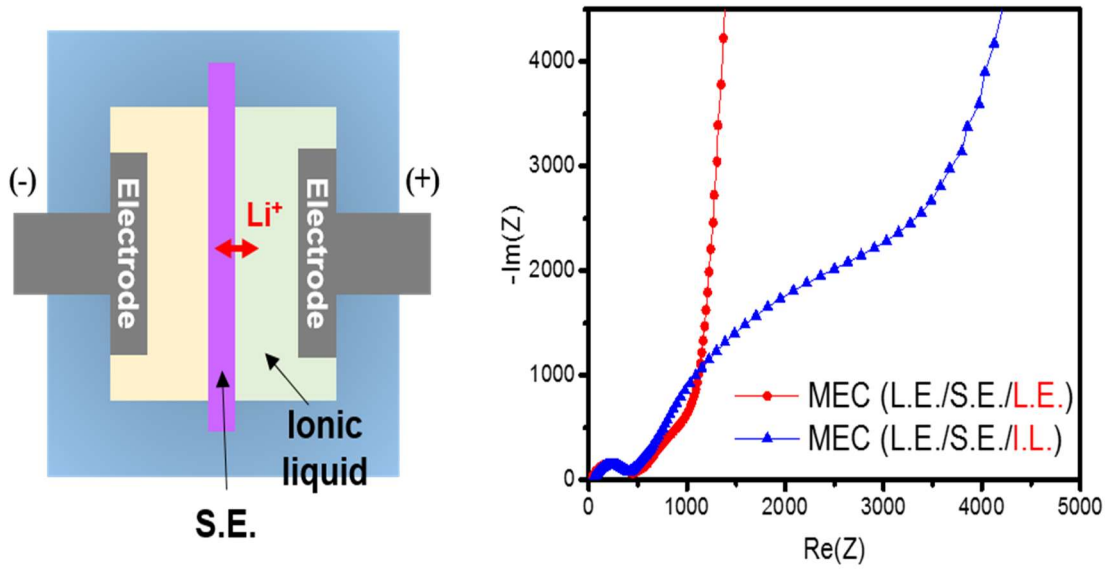

Figure 1.16 Electrochemical impedance spectroscopy for Multi-layer electrolyte cell (1.0M $LiPF_6$ in EC:DMC (1:1vol/vol) / Solid electrolyte / 0.1mol% LiTFSI in Py_{14}TFSI) without active material.

ULSAN NATIONAL INSTITUTE OF SCIENCE AND TECHNOLOGY

There is other data to confirm the multi-layer electrolyte cell`s properties using $LiCoO_2$, $LiFePO_4$ materials as shown in fig. 1.17. These cells operate reasonably at room temperature low C-rate 1/40 C, 1/30 C respectively. But, there is large polarization in case of increase of the C-rate. The ionic liquids have commonly high viscosity to affect ion conductivity and interfacial resistance between solid electrolytes and ionic liquids.

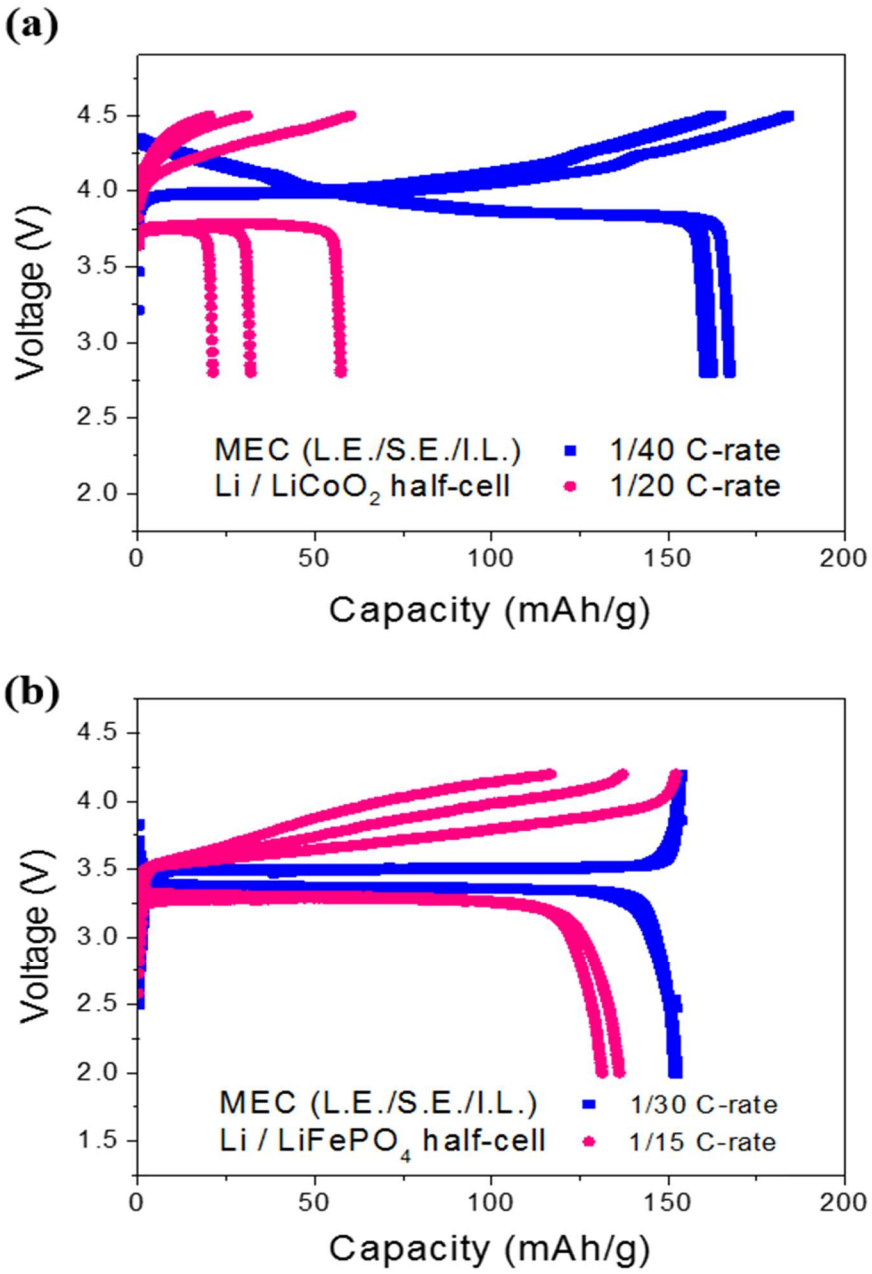

Figure 1.17 Voltage profile for Multi-layer electrolyte cell (1.0M $LiPF_6$ in EC:DMC (1:1vol/vol%) / S.E. / 0.1mol% LiTFSI in $Py_{14}TFSI$) cycling (a) Li / $LiCoO_2$ half-cell, (b) Li / $LiFePO_4$ half-cell at room temperature.

ULSAN NATIONAL INSTITUTE OF SCIENCE AND TECHNOLOGY

To reduce the internal resistance of the multi-layer electrolyte cell, we prepared the solid electrolyte $Li_{1.3}Ti_{1.7}Al_{0.3}(PO_4)_3$ with porosity that could expand the contact surface with ionic liquid electrolyte. The ionic liquid electrolytes were inserted into the porosity of the pellet to broaden area and reduce interfacial resistance between ionic liquid and solid electrolyte. To make the porosity on the pellet, we prepared a mixture pellet of LTAP powders and LTAP precursors with specific ratios. When we synthesized the porous LTAP pellet, LTAP precursors left the porosity on the pellet. As seen in figure 1.18, TGA shows that 16 wt% percentage of the mixture pellet evaporates. SEM image inserted in fig. 1.18 also shows the surface`s difference between pellets. Physisorption analyzer measures the total pore volume of ceramic electrolyte pellet. The porous LTAP pellet has 1000 times wider pore volume than that of OHARA LTAP pellet. (8.16×10^{-3} cm^3/g and 3.76×10^{-6} cm^3/g respectively) The ionic liquids are impregnated into the porous pellet and reduce the resistance of the MEC.

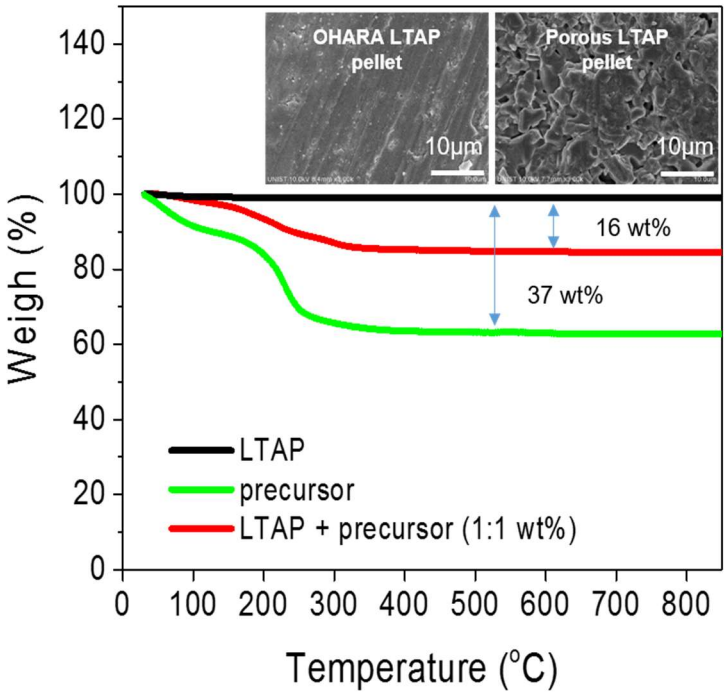

Figure 1.18 (a) Thermogravimetric analysis of OHARA LTAP pellet, precursor and mixed pellet inserted SEM images of OHARA LTAP pellet and porous LTAP pellet.

ULSAN NATIONAL INSTITUTE OF SCIENCE AND TECHNOLOGY

As seen in figure 1.19 (a), the porous pellet type MEC has lower resistance than that of previous MEC model 1. Especially, the second large semi-circle of former MEC decreased very much. We consider that the interfacial resistance between ceramic electrolyte pellet and ionic liquid is important because the second semi-circle of the OHARA pellet type MEC model 1 decreases when pellet is replaced with porous pellet. That means porosity of the pellet contains the ionic liquid and helps LTAP pellet reduce that interface resistance between pellet and ionic liquid. Figure 1.19

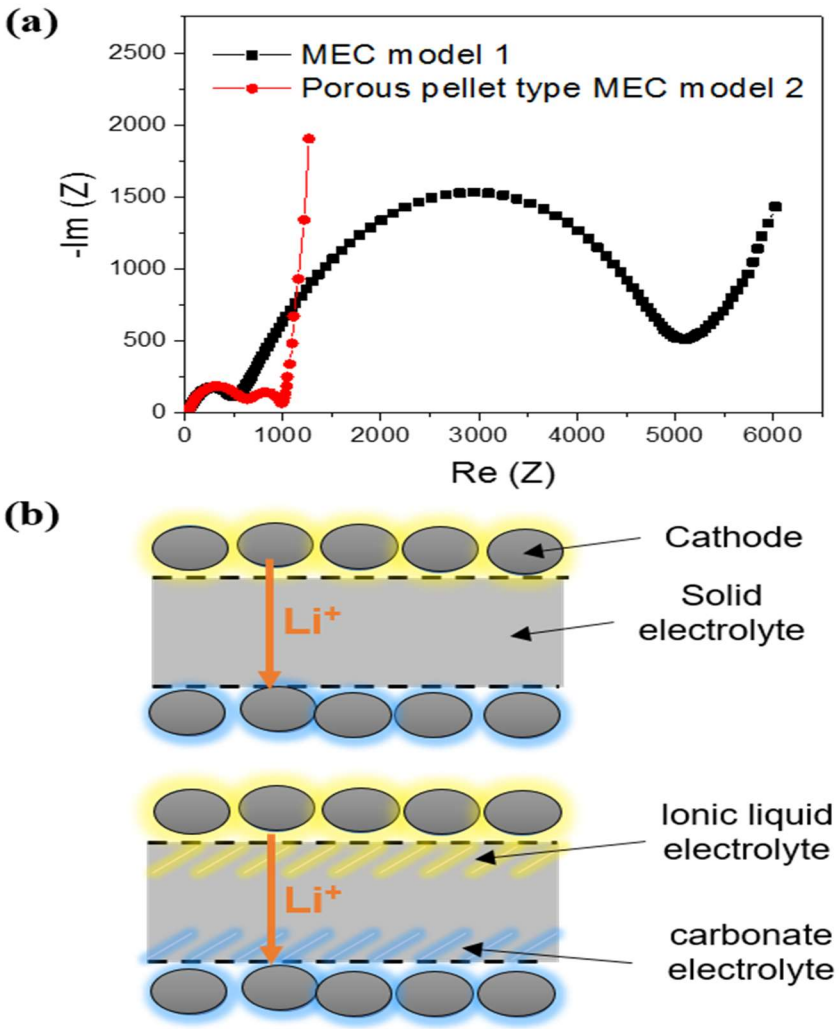

Figure 1.19 (a) Electrochemical impedance spectroscopy for three type multi-layer electrolyte cells of Li / $Li_{1.2}Ni_{0.15}Mn_{0.55}Co_{0.1}O_2$ (b) schematic ion conducting pathway throughout multi-layer electrolyte cell. (b) shows schematically the viscous ionic liquid defined in cathode compartment is not compatible with sleek OHARA LTAP pellet. However, porous LTAP pellet have wider surface area to contact with ionic liquid and reduce the resistance.

ULSAN NATIONAL INSTITUTE OF SCIENCE AND TECHNOLOGY

The porous LTAP pellet type multi-layer electrolyte cell has higher capacity because it has lower internal resistance than that of previous MEC model 1. As seen in figure 1.20, porous type MEC shows capacity over 250 mAh/g, which is comparable to that of coin cell using carbonate- base electrolyte. The carbonate electrolyte containing $LiPF_6$ is oxidized easily at high voltage as shown in figure 1.12 (a) and negatively influences the charge / discharge curve in figure 1.13. Operating the cell at elevated temperatures activates the Li_2MnO_3 component in the cathode materials and delivers more capacities. But, these harsh conditions accelerate the oxidation decomposition of the electrolyte and consume reversible Li^+ ion. The large charge capacity and low coulombic efficiency suggest that carbonate electrolytes are oxidized. the porous type MEC has large capacity and good coulombic efficiency that means reversible electrochemical reaction occurs at cathode materials. Although multi-layer electrolyte cell improved the electrolyte`s stability at high potential, there is capacity and voltage fading during cycle because of compositional phase change of the over-lithiated layered oxide materials[55].

To identify the effect of the multi-layer electrolyte (L.E./S.E./I.L.) compared to ionic liquid electrolyte, test coin half-cell using only the Py_{14} TFSI ionic liquid electrolyte at same condition shown as figure 1.21. The coin cell showed a high charge and discharge capacity at first cycle comparable to multi-layer electrolyte cell (L.E./S.E./I.L.), but the voltage curve of the second cycle had deceased during cycling. It is supposed that ceramic solid electrolyte $Li_{1.3}Ti_{1.7}Al_{0.3}(PO_4)_3$ pellet stabilizes the cell in harsh conditions and prevents the electrolytes being blended and crossover of the decomposition product.

ULSAN NATIONAL INSTITUTE OF SCIENCE AND TECHNOLOGY

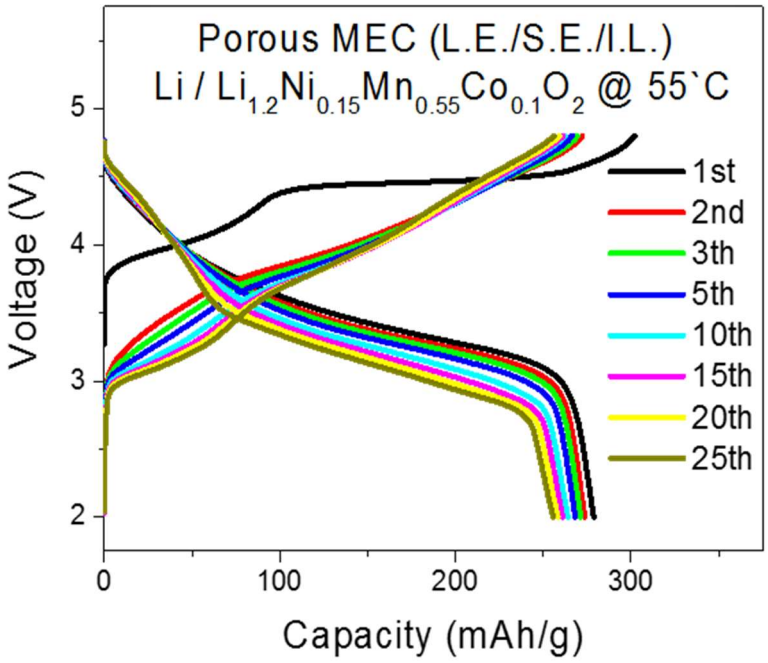

Figure 1.20 Charge and discharge voltage profile for porous pellet type multi-layer electrolyte cell (1.0M $LiPF_6$ in EC:DMC (1:1vol/vol%) / S.E. / 0.1mol% LiTFSI in $Py_{14}TFSI$) of Li / $Li_{1.2}Ni_{0.15}Mn_{0.55}Co_{0.1}O_2$ at C/20 rate and 55ºC.

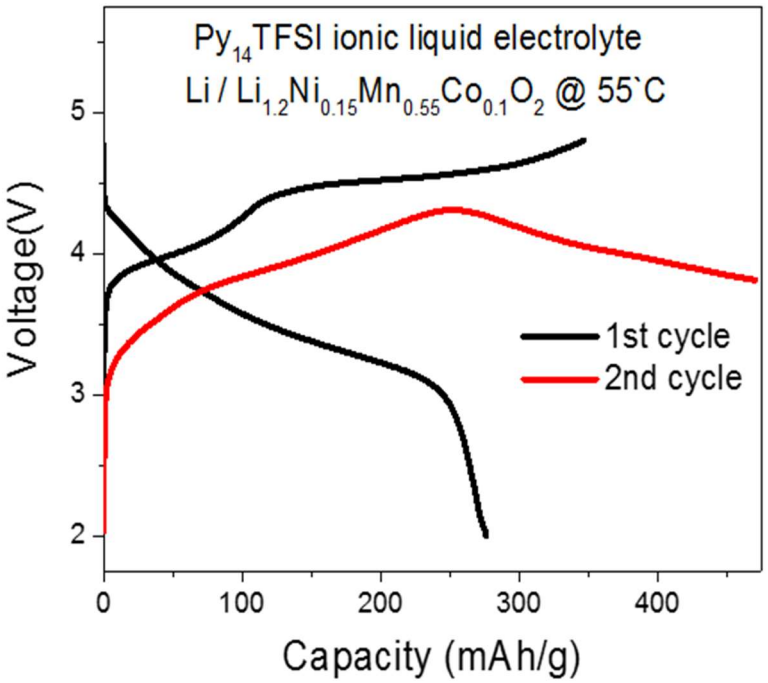

Figure 1.21 Charge and discharge voltage profile for ionic liquid electrolyte half-cell ($Py_{14}TFSI$) of Li / $Li_{1.2}Ni_{0.15}Mn_{0.55}Co_{0.1}O_2$ at C/20 rate and 55ºC.

ULSAN NATIONAL INSTITUTE OF SCIENCE AND TECHNOLOGY

1.8 Conclusion

Multi-layer electrolyte cell (MEC) was designed to improve the stability of the electrolyte at high voltage and elevated temperature. Linear sweep voltammetry studies confirmed that ionic liquid electrolyte has higher potential stability than that of carbonate-based electrolyte. MEC (L.E./S.E./I.L.) improved the stability of Li / $Li_{1.2}Ni_{0.15}Mn_{0.55}Co_{0.1}O_2$ half-cell at high voltage and elevated temperature. But, the solid electrolyte $Li_{1.3}Ti_{1.7}Al_{0.3}(PO_4)_3$ which is used in MEC has high interface resistance between ceramic electrolyte pellet and ionic liquid electrolyte. The porous solid electrolyte broadens the contact surface area with ionic liquid electrolyte, which reduces the interfacial resistance between them. The porous pellet type MEC of Li / $Li_{1.2}Ni_{0.15}Mn_{0.55}Co_{0.1}O_2$ half-cell has comparable capacity and high stability at high voltage and elevated temperature. MEC designs have intrinsic high internal resistance compared to commercial LIB, so the solid electrolyte should develop their ionic conductivity and good interfacial resistance.

ULSAN NATIONAL INSTITUTE OF SCIENCE AND TECHNOLOGY

Chapter 2.

2 Next generation Multi-layer electrolyte for high energy density Li-ion battery

2.1 Solid electrolyte interphase (SEI layer) formation on graphite anode

The electrochemical stability window of the carbonate-based liquid electrolyte is lower than the potential of graphite anode, causing a reduction in the decomposition reaction of the electrolyte shown as figure 1.2. The solid electrolyte interphase (SEI layer) on the surface of the graphite anode is formed to prevent further decomposition reaction during first decomposition of the electrolyte. But, SEI layer formation of graphite anode is an obstacle to realization of high energy density LIB because it consumes the Li^+ ions and capacity which could be delivered reversibly within LIB. This consumption of Li^+ ions reduces the reversible capacity of the LIB full-cell and parts of cathode materials which should contribute high potential as shown in figure 2.1 [56,57,58]. Therefore, by inserting ceramic electrolytes, lithium source additives, that can provide additional Li^+ ions to increase the initial capacity, the capacity of the LIB is restored and maximizes the cathode materials to utilize for high energy LIB. After that, the ceramic electrolyte has wide application to LIB functioned as the ionic conductive solid electrolyte [59].

2.2 Ceramic electrolyte candidates for lithium source material

The lithium source additives candidate group should have redox potential of 2.5V ~ 1.0 V vs. Li/Li^+ to be inactive at LIB full-cell operating voltage 4.2V ~ 2.5V like blue box area in figure 2.1 (d). Sulfide and oxide series materials are included among lithium source additive candidates. As seen figure 2.2 (a) and (b), sulfide-based materials have a high-energy level of

ULSAN NATIONAL INSTITUTE OF SCIENCE AND TECHNOLOGY

sulfur $3P^6$ orbital, which causes decomposition of sulfide material at high voltage 3.0 V vs. Li/Li^+. On the other hand, oxygen $2P^6$ orbital of oxide material is stable at high potential because it has a higher energy level than 4.2V vs. Li/Li^+ in figure 2.2 (b).

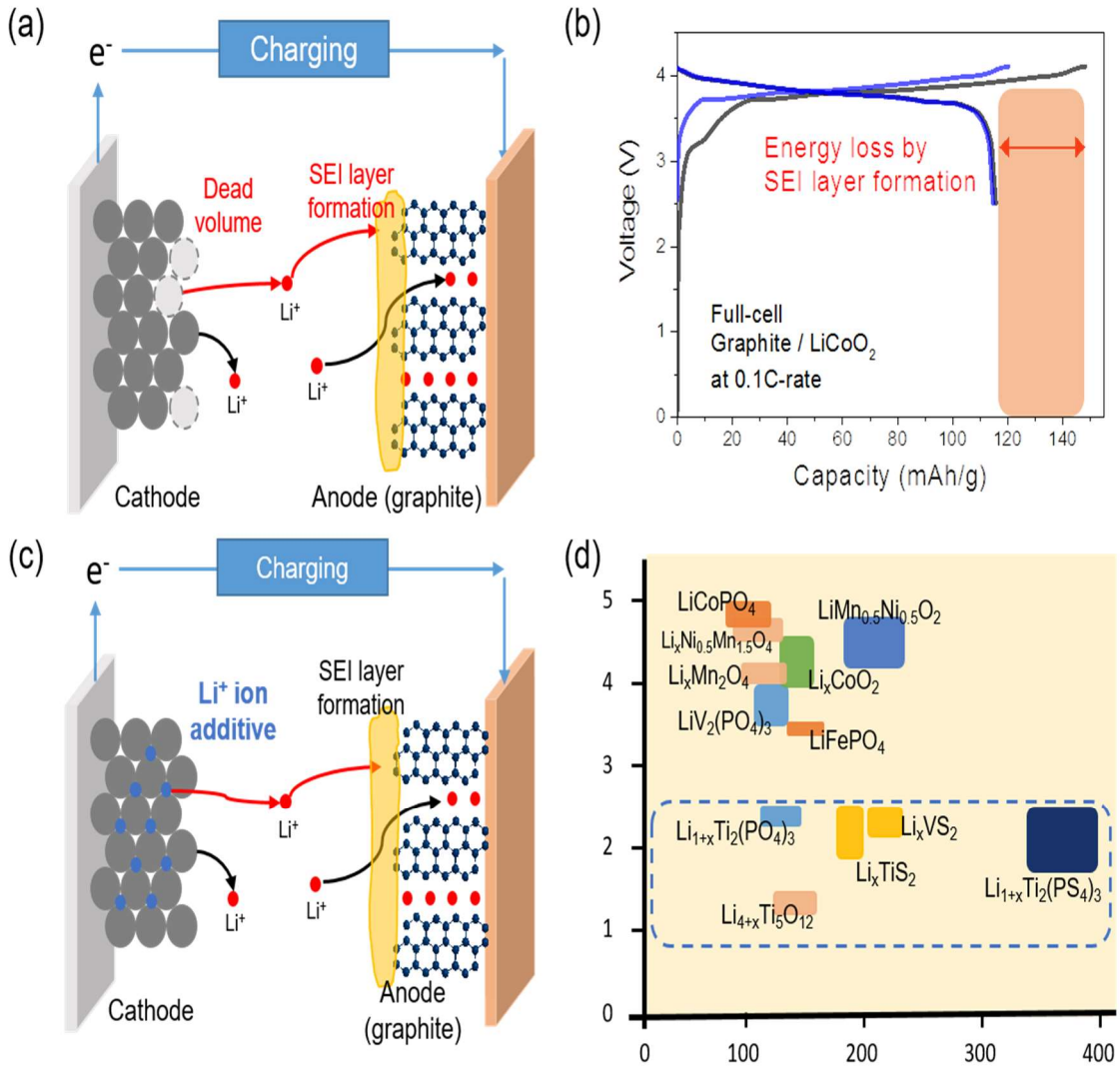

Figure 2.1 (a) SEI layer formation consumes the Li ions causing dead volume of the cathode materials (b) reduction of the capacity limited in full-cell by SEI layer formation (c) Lithium source additives compensate the capacity consumed by SEI layer formation, which leads the cathode materials utilized at the max (d) lithium source additive candidates and conditions for the additive.

ULSAN NATIONAL INSTITUTE OF SCIENCE AND TECHNOLOGY

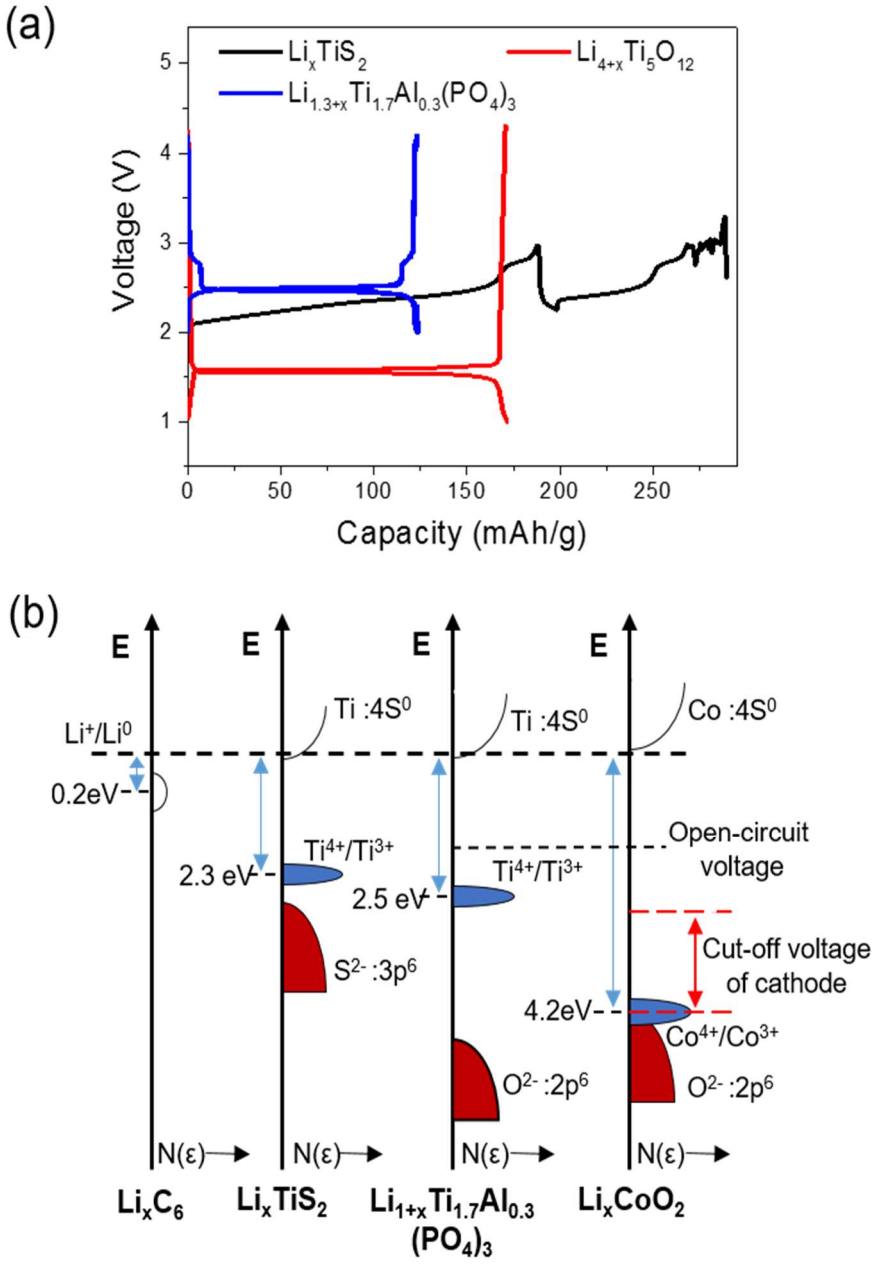

Figure 2.2 (a) Voltage profile showing the capacity, redox potential and stability of the lithium source additive at high voltage (b) Schematic of their corresponding energy vs. density of states describing Li^+ ions contribution and the stability of the candidate at high voltage.

ULSAN NATIONAL INSTITUTE OF SCIENCE AND TECHNOLOGY

Lithium source materials, $Li_{1.3+1.7}Ti_{1.7}Al_{0.3}(PO_4)_3$ have open-circuit voltage (OCV) 2.4V vs. Li/Li^+ and provide the additional 1.7 mole of Li^+ ions per 1 mole of $Li_{1.3+1.7}Ti_{1.7}Al_{0.3}(PO_4)_3$ to graphite anode during charging process, which minimizes the dead volume of the cathode materials. After charge process, $Li_{1.3}Ti_{1.7}Al_{0.3}(PO_4)_3$ (LTAP) materials does not react electrochemically as electrode in cut-off voltage and function as solid electrolyte which has ion conductivity 1.9 x 10^{-4} S/cm as shown in figure 1.11.

$Li_4Ti_5O_{12}$, LTAP materials can be used in oxide materials. LTAP materials have ionic conductivity, which could provide ion-pathway inside cell. Since LTAP materials are lithium deintercalated materials, lithium intercalated materials which have same structure must be synthesized in advance. Therefore, we made lithium intercalated materials chemically and identified the properties of the material.

2.2 Experiment

$LiTiS_2$, $Li_4Ti_5O_{12}$, LTAP were used as candidates of lithium source additive. The LTAP powders were synthesized according to previous chapter 1. Lithium intercalation $Li_{1.3+1.7}Ti_{1.7}Al_{0.3}(PO_4)_3$ powders were obtained by reaction of $Li_{1.3}Ti_{1.7}Al_{0.3}(PO_4)_3$ powders and n-butyl lithium in hexane solution in excess as shown in figure 2.3 [60,61]. Filtered and washed the product with hexane. The slurry of lithium source additives material 80wt%, super P 10wt% and PvdF 10wt% was loaded on an aluminum current collector. Lithium intercalation material was blended with cathode materials in some ratio.

A 2032-type coin cell was employed to assess the electrochemical performance of the lithium source full-cell. 1.0 M $LiPF_6$ dissolved in a mixture of ethylene carbonate (EC), diethylcarbonate (DEC) (1:1 vol/vol) was fabricated as electrolytes. Porous 20 μm thick polyethylene (PE) film was used as the separator. All the processes for fabricating the

ULSAN NATIONAL INSTITUTE OF SCIENCE AND TECHNOLOGY

composite electrode and assembling the coin cells were carried out in the Ar-filled glove box. Full-cells with graphite/$LiCoO_2$ (reference), graphite/$LiCoO_2$ blended with lithium source were assembled.

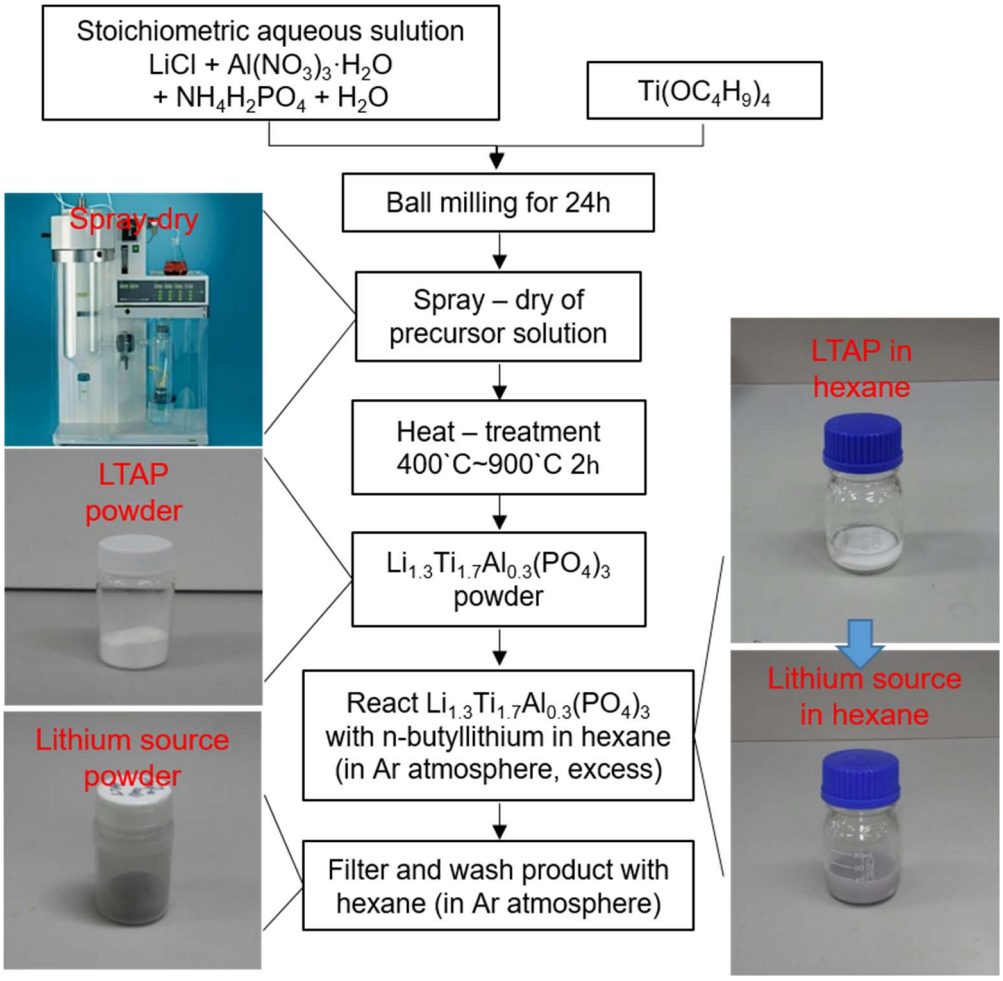

Figure 2.3 Preparation of lithium source material $Li_{1.3+1.7}Ti_{1.7}Al_{0.3}(PO_4)_3$

ULSAN NATIONAL INSTITUTE OF SCIENCE AND TECHNOLOGY

2.3 Result and Discussion

For testing of $LiTiS_2$ sulfide materials to use lithium source additive at high voltage, $Li/LiTiS_2$ half-cells were measured under cut-off voltage of 4.2V to 2.0V. Since the sulfur $3P^6$ orbital of the $LiTiS_2$ material has a high-energy level, it decomposed irreversibly above 3.5V shown in figure 2.2 (a). When applied to the cathode side of full-cell, there was long charge reaction during decomposition of sulfide material. Therefore, it is difficult to use sulfide materials which has low high voltage stability as lithium source.

Oxide series include spinel structure $Li_4Ti_5O_{12}$, NASICON-type structure LTAP materials. The lithium intercalation material $Li_{4+3}Ti_5O_{12}$ of deintercalation materials $Li_4Ti_5O_{12}$ is difficult

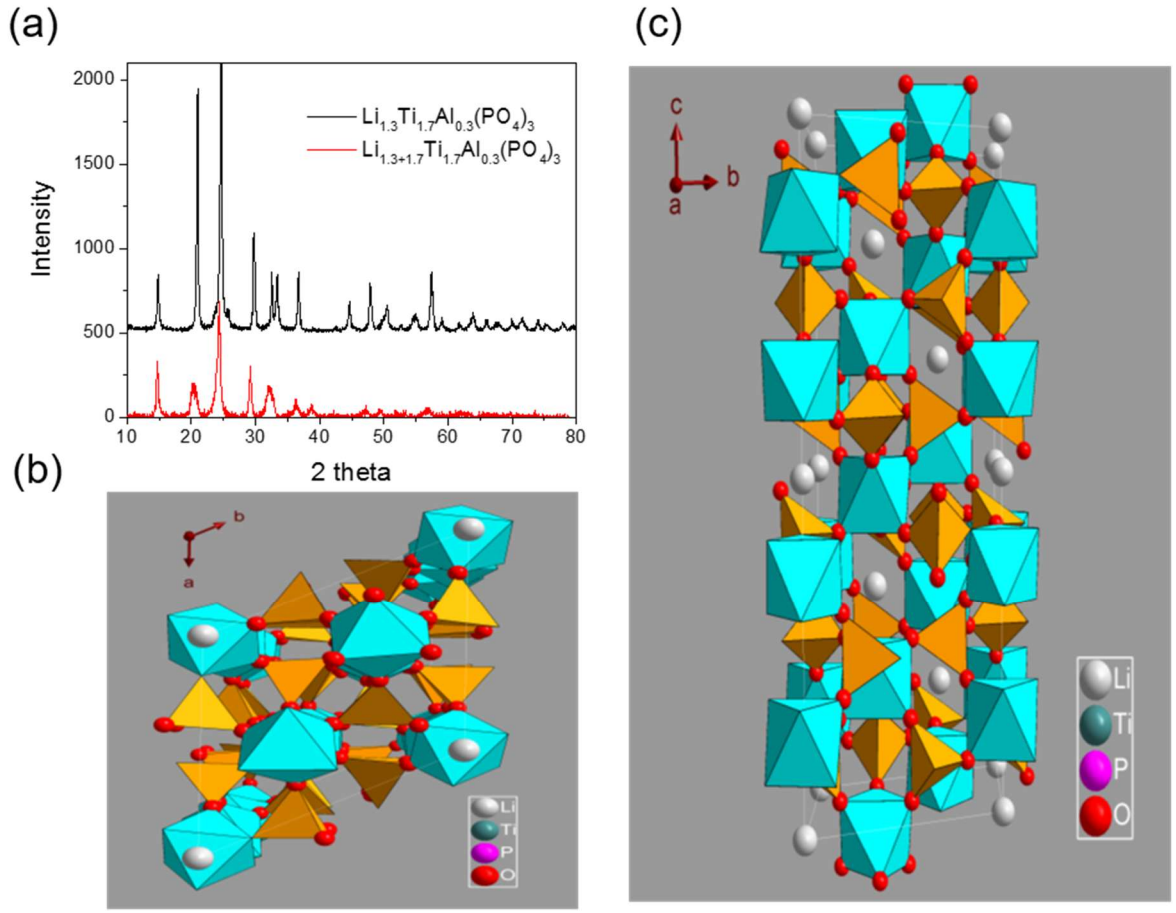

Figure 2.4 (a) Powder X-ray diffraction pattern of the $Li_{1.3}Ti_{1.7}Al_{0.3}(PO_4)_3$ and $Li_{1.3+1.7}Ti_{1.7}Al_{0.3}(PO_4)_3$ (b), (c) crystal structure of NASICON – type $Li_{1.3}Ti_{1.7}Al_{0.3}(PO_4)_3$ by z, x axis respectively.

ULSAN NATIONAL INSTITUTE OF SCIENCE AND TECHNOLOGY

to chemically synthesize because of the higher the energy level, the lower the stability of the Li intercalation material. On other hand, NASICON-type structure material is easy to make easily into lithium intercalation materials. Furthermore, LTAP material possesses the highest ionic conductivity among various substituents of the NASICON-type structure. It is significant that lithium source additives are ion conducting materials. These additives should block the Li^+ ion pathways throughout cell. However, LTAP materials transfers Li^+ ions to the other electrode smoothly. Figure 2.4 shows that powder X-ray diffraction pattern of the ground $Li_{1.3}Ti_{1.7}Al_{0.3}(PO_4)_3$ material, Li-rich $Li_{1.3+1.7}Ti_{1.7}Al_{0.3}(PO_4)_3$ material. The LTAP material can perform Li intercalation/deintercalation reaction as an electrode material as well as an Li^+ ion conducting solid electrolyte. It has two Li sites M1, M2 of NAISCON-type structure as shown in figure 2.4 (b), (c). The M1 site is occupied by existing Li^+ ions. Additional Li^+ ions can be inserted into vacant M2 site.

To chemically synthesize $Li_{1.3+1.7}Ti_{1.7}Al_{0.3}(PO_4)_3$, LTAP powder and n-butyl lithium solution were reacted in Ar atmosphere. We have synthesized $Li_{1.3+1.7}Ti_{1.7}Al_{0.3}(PO_4)_3$ occupied with additional Li^+ ion into vacancy M2 Li site of LTAP material. Figure 2.5 (a) shows that the ionic conductivity of $Li_{1.3+1.7}Ti_{1.7}Al_{0.3}(PO_4)_3$ decreases because the vacant Li sites M2 are filled with extra Li^+ ions. It is reasonable that sites filled with Li^+ ions in the structure cannot conduct Li^+ ions faster than before. After delithiation of the lithium source materials, the ionic conductivity of $Li_{1.3}Ti_{1.7}Al_{0.3}(PO_4)_3$ material in figure 2.5 (b) is 1.9×10^{-4} S/cm at room temperature. It is expected to help ionic conduction as solid electrolyte after delithiation from lithium source. Half-cell with synthesized $Li_{1.3+1.7}Ti_{1.7}Al_{0.3}(PO_4)_3$ shows open-circuit voltage (OCV) 2.1V vs. Li/Li^+ in figure 2.5 (c). This indicates that Li intercalation has worked well. However, when this material electrode is exposed to air, the OCV rises and the amount of Li deintercalation is greatly reduced. It was tested at a very low current of 1/40 C-rate. The initial charge capacity of $Li_{1.3+1.7}Ti_{1.7}Al_{0.3}(PO_4)_3$ was more than 110 mAh/g[54], which was slightly lower than

ULSAN NATIONAL INSTITUTE OF SCIENCE AND TECHNOLOGY

theoretical capacity, but the amount of Li intercalation can be utilized for additive. This material satisfies qualifications for lithium source; operating voltage at 2.5V Li/Li^+ and stability at 4.2V vs. Li/Li^+ without side-reaction. Figure 2.5 (d) shows that $Li_{1.3+1.7}Ti_{1.7}Al_{0.3}(PO_4)_3$ material has poor C-rate capabilities of 1/20 C-rate. It has low initial charge capacity, 80 mAh g^{-1}, meaning probably provides less Li^+ ions to SEI layer formation at 1/20 C-rate.

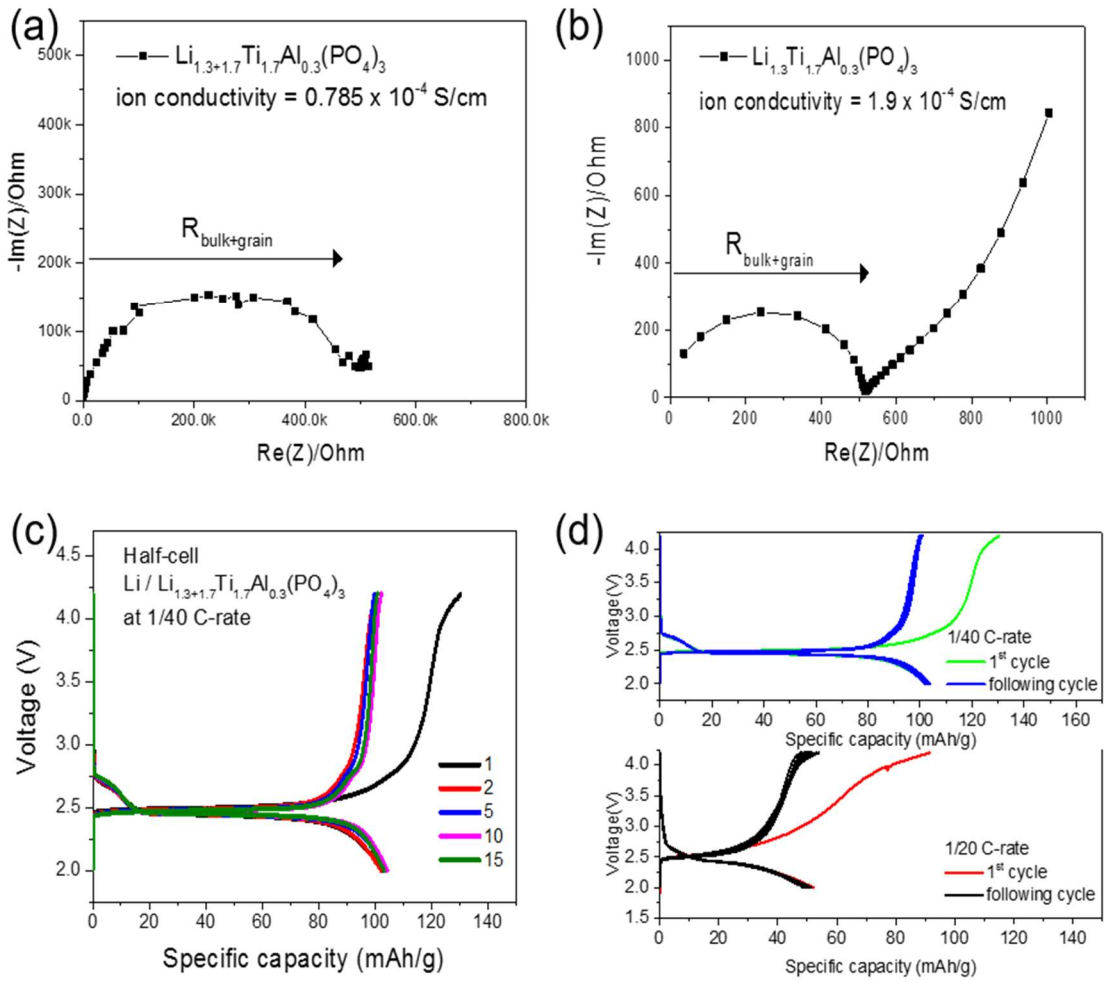

Figure 2.5 Ionic conductivity of (a) lithium source additive $Li_{1.3+1.7}Ti_{1.7}Al_{0.3}(PO_4)_3$ and (b) ceramic electrolyte $Li_{1.3}Ti_{1.7}Al_{0.3}(PO_4)_3$ (c) charge/discharge voltage profile (d) C-rate capabilities of 1/40 C-rate and 1/20 C-rate Li / $Li_{1.3+1.7}Ti_{1.7}Al_{0.3}(PO_4)_3$ half-cell.

ULSAN NATIONAL INSTITUTE OF SCIENCE AND TECHNOLOGY

We designed Graphite / $LiCoO_2$ full cell with N/P ratio of 1.2. The SEI layer on the graphite is formed during the first charge, which of the amount is examined with reference cell. We compensate the Li^+ ion consumption, capacity, by blending lithium source additives with cathode materials. The delithiation of $Li_{1.3+1.7}Ti_{1.7}Al_{0.3}(PO_4)_3$ shows charge capacity from 1.5 V in full cell. This $Li_{1.3+1.7}Ti_{1.7}Al_{0.3}$ $(PO_4)_3$ material contributes Li^+ ion in the first charge cycle and is inactive in subsequent cycles. Compared to the same N/P ratio graphite/LCO reference cell, more reversible capacity is secured in the initial and following cycle of full-cell as shown in figure 2.6 (a), (c). Figure 2.6 (b) shows the contribution of lithium source during SEI layer

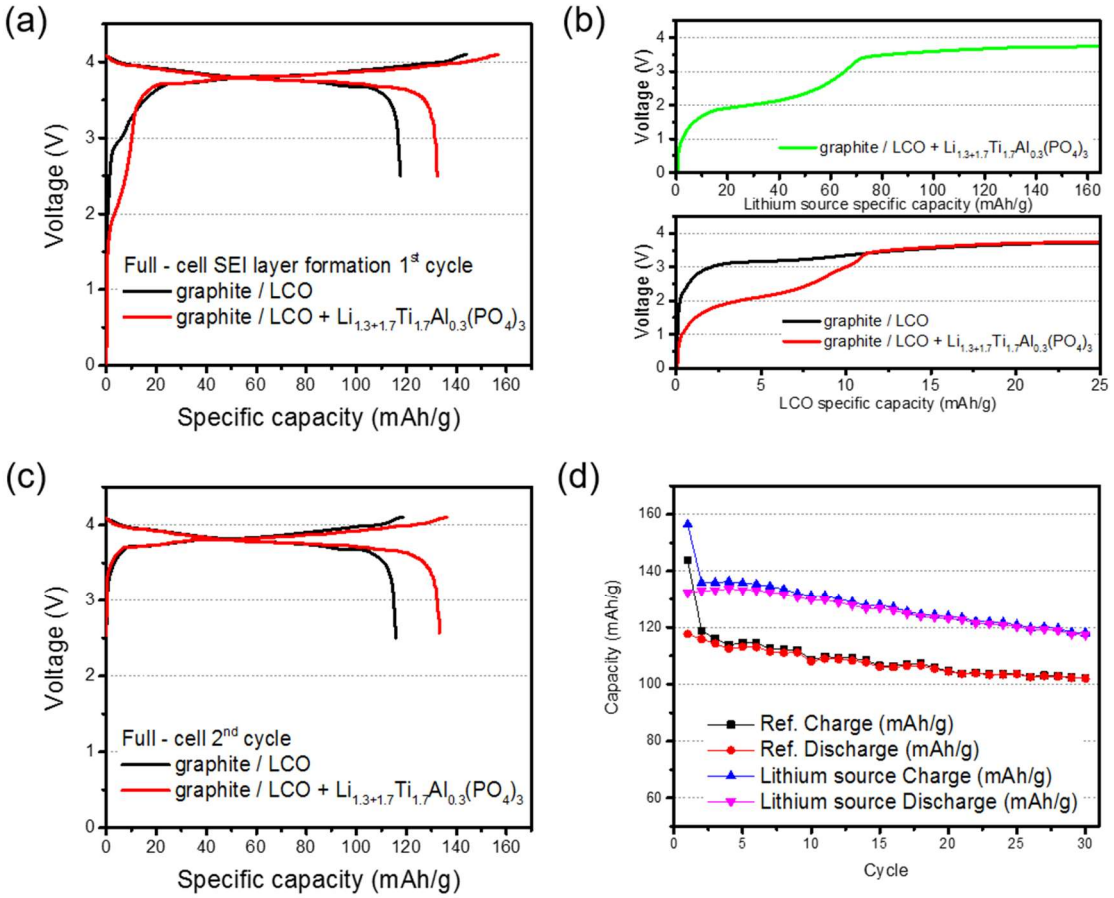

Figure 2.6 (a) Initial full cell cycle performance of pristine and the mixed $Li_{1.3+1.7}Ti_{1.7}Al_{0.3}(PO_4)_3$ with $LiCoO_2$ cathode at C/20 rate. The anode is the graphite. (b) magnifying initial charge capacity provided by lithium source (c) subsequent cycle of them at C/10 rate. (d) The corresponding charge/discharge performances cycled at C/20 for initial two cycles and C/10 for the subsequence cycles.

ULSAN NATIONAL INSTITUTE OF SCIENCE AND TECHNOLOGY

formation. We calculate the specific capacity of $LiCoO_2$ cathode material, $Li_{1.3+1.7}Ti_{1.7}Al_{0.3}(PO_4)_3$ material respectively to identify contribution of lithium source. At initial charge process, lithium source provides additional capacity of about 65 mAh/g of $Li_{1.3+1.7}Ti_{1.7}Al_{0.3}(PO_4)_3$ specific capacity. This is coincident that $Li_{1.3+1.7}Ti_{1.7}Al_{0.3}(PO_4)_3$ material has poor C-rate capability of 1/20 C-rate. The increase of reversible capacity could be confirmed in figure 2.6 (d).

ULSAN NATIONAL INSTITUTE OF SCIENCE AND TECHNOLOGY

2.4 Conclusions

The graphite anode forms the SEI layer (Solid electrolyte interphase) consuming the reversible lithium ion in LIB because the electrochemical stability window of electrolyte is higher than redox potential of graphite. The ceramic electrolyte $Li_{1.3}Ti_{1.7}Al_{0.3}(PO_4)_3$ (LTAP) materials provides additional lithium source to recover the capacity of LIB full-cell. They have NASICON – type structure of two Li sites M1, M2. The M1 site is occupied by existing Li^+ ions, additional Li^+ ions can be inserted into vacant M2 site. Li rich $Li_{1.3+1.7}Ti_{1.7}Al_{0.3}(PO_4)_3$ materials are synthesized chemically and used by lithium source in LIB full-cell. When lithiation in NASICON – structure, Li rich $Li_{1.3+1.7}Ti_{1.7}Al_{0.3}(PO_4)_3$ has lower ionic conductivity than that of before. However, after the first charge cycle, LTAP has ionic conductivity 10^{-4} S/cm, so it is help lithium ion conduct inside cell. LTAP materials provide an additional lithium source ofabout 110 mAh/g. The contribution of lithium source material is confirmed by applying to graphite / $LiCoO_2$ full-cell. To achieve higher capacity, ceramic electrolyte materials that have higher capacity could be applied.

ULSAN NATIONAL INSTITUTE OF SCIENCE AND TECHNOLOGY

References

1. IEC. Executive summary. *Electr. Energy Storage White Pap.* **39,** 11–12 (2009).
2. Asl, N. M. *et al.* Purdue university. **9,**
3. Goodenough, J. B. & Kim, Y. Challenges for Rechargeable Li Batteries †. *Chem. Mater.* **22,** 587–603 (2010).
4. Park, O. K. *et al.* Who will drive electric vehicles, olivine or spinel? *Energy Environ. Sci.* **4,** 1621 (2011).
5. Gnanaraj, J. S., Pol, V. G., Gedanken, A. & Aurbach, D. Improving the high-temperature performance of LiMn2O 4 spinel electrodes by coating the active mass with MgO via a sonochemical method. *Electrochem. commun.* **5,** 940–945 (2003).
6. Choi, N., Han, J. & Ha, S. RSC Advances stability of high-voltage cathodes in lithium-ion. *RSC Adv.* **5,** 2732–2748 (2014).
7. Choa, J. & Thackeray, M. M. Structural Changes of LiMn2 O 4 Spinel Electrodes during Electrochemical Cycling. *J. Electrochem. Soc.* **146,** 3577–3581 (1999).
8. Benedek, R. & Thackeray, M. M. Reaction Energy for LiMn2O4 Spinel Dissolution in Acid. *Electrochem. Solid-State Lett.* **9,** A265 (2006).
9. Tsunekawa, H. *et al.* Capacity Fading of Graphite Electrodes Due to the Deposition of Manganese Ions on Them in Li-Ion Batteries. *J. Electrochem. Soc.* **149,** A1326 (2002).
10. Cho, I. H., Kim, S.-S., Shin, S. C. & Choi, N.-S. Effect of SEI on Capacity Losses of Spinel Lithium Manganese Oxide/Graphite Batteries Stored at 60°C. *Electrochem. Solid-State Lett.* **13,** A168 (2010).
11. Mahootcheianasl, N., Kim, J. H., Pieczonka, N. P. W., Liu, Z. & Kim, Y. Multilayer electrolyte cell: A new tool for identifying electrochemical performances of high voltage cathode materials. *Electrochem. commun.* **32,** 1–4 (2013).
12. Bachman, J. C. *et al.* Inorganic Solid-State Electrolytes for Lithium Batteries: Mechanisms and Properties Governing Ion Conduction. *Chem. Rev.* **116,** 140–162 (2016).
13. Abrahams, I., Bruce, P. G., West, A. R. & David, W. I. F. Structure determination of LISICON solid solutions by powder neutron diffraction. *J. Solid State Chem.* **75,** 390–396 (1988).
14. Hong, H. Y. P. Crystal structure and ionic conductivity of Li14Zn(GeO4)4 and other new Li+ superionic conductors. *Mater. Res. Bull.* **13,** 117–124 (1978).
15. Bruce, P. G. The A-C Conductivity of Polycrystalline LISICON, Li[sub 2+2x]Zn[sub 1−x]GeO[sub 4], and a Model for Intergranular Constriction Resistances. *J. Electrochem. Soc.* **130,** 662 (1983).
16. Robertson, A. ., West, A. . & Ritchie, A. . Review of crystalline lithium-ion conductors suitable for high temperature battery applications. *Solid State Ionics* **104,** 1–11 (1997).
17. Goodenough, J. B., Hong, H. Y. & Kafalas, J. A. R. G. Graves and J. B. Smathers. **5,** 77843 (1976).
18. Fu, J. Superionic conductivity of glass-ceramics in the system Li2O_ Al2O3_TiO2_P2O5. *Solid State Ionics* **96,** 195–200 (1997).
19. Mariappan, C. R., Gellert, M., Yada, C., Rosciano, F. & Roling, B. Grain boundary resistance of fast lithium ion conductors: Comparison between a lithium-ion conductive Li-Al-Ti-P-O-type glass ceramic and a Li 1.5Al0.5Ge1.5P3O12 ceramic. *Electrochem. commun.* **14,** 25–28 (2012).
20. Takahashi, K. *et al.* A Super High Lithium Ion Conducting Solid Electrolyte of Grain Boundary Modified Li1.4Ti1.6 Al0.4(PO4)3. *J. Electrochem. Soc.* **159,** A342 (2012).
21. Inaguma, Y. *et al.* High ionic conductivity in lithium lanthanum titanate. *Solid State*

ULSAN NATIONAL INSTITUTE OF SCIENCE AND TECHNOLOGY

Commun. **86,** 689–693 (1993).
22. Knauth, P. Inorganic solid Li ion conductors: An overview. *Solid State Ionics* **180,** 911–916 (2009).
23. Thangadurai, V. & Weppner, W. Recent progress in solid oxide and lithium ion conducting electrolytes research. *Ionics (Kiel).* **12,** 81–92 (2006).
24. Inaguma, Y. & Itoh, M. Influences of carrier concentration and site percolation on lithium ion conductivity in perovskite-type oxides. *Solid State Ionics* **86–88,** 257–260 (1996).
25. García-Martín, S., Alario-Franco, M. A., Ehrenberg, H., Rodríguez-Carvajal, J. & Amador, U. Crystal Structure and Microstructure of Some La2/3-xLi3xTiO3 Oxides: An Example of the Complementary Use of Electron Diffraction and Microscopy and Synchrotron X-ray Diffraction To Study Complex Materials. *J. Am. Chem. Soc.* **126,** 3587–3596 (2004).
26. Thangadurai, V., Narayanan, S. & Pinzaru, D. Garnet-type solid-state fast Li ion conductors for Li batteries: critical review. *Chem. Soc. Rev.* **43,** 4714 (2014).
27. Wang, W. G. *et al.* Internal friction study on the lithium ion diffusion of Li 5 La 3 M 2 O 12 (M ¼ Ta , Nb) ionic conductors. **13,** 1760–1764 (2011).
28. Murugan, R., Thangadurai, V. & Weppner, W. Fast lithium ion conduction in garnet-type Li7La 3Zr2O12. *Angew. Chemie - Int. Ed.* **46,** 7778–7781 (2007).
29. Thangadurai, V., Pinzaru, D., Narayanan, S. & Baral, A. K. Fast Solid-State Li Ion Conducting Garnet-Type Structure Metal Oxides for Energy Storage. *J. Phys. Chem. Lett.* **6,** 292–299 (2015).
30. Cussen, E. J. Structure and ionic conductivity in lithium garnets. *J. Mater. Chem.* **20,** 5167–5173 (2010).
31. Bulut, S. *et al.* Temperature dependence of the viscosity and conductivity of mildly functionalized and non-functionalized [Tf2N](-) ionic liquids. *Chemphyschem* **12,** 2296–2310 (2011).
32. Hayyan, M., Mjalli, F. S., Hashim, M. A., AlNashef, I. M. & Mei, T. X. Investigating the electrochemical windows of ionic liquids. *J. Ind. Eng. Chem.* **19,** 106–112 (2013).
33. Zhang, S., Sun, N., He, X., Lu, X. & Zhang, X. Physical properties of ionic liquids: Database and evaluation. *J. Phys. Chem. Ref. Data* **35,** 1475–1517 (2006).
34. Li, J., Jeong, S., Kloepsch, R., Winter, M. & Passerini, S. Improved electrochemical performance of LiMO2 (M=Mn, Ni, Co)-Li2MnO3 cathode materials in ionic liquid-based electrolyte. *J. Power Sources* **239,** 490–495 (2013).
35. Zheng, J., Zhu, D., Yang, Y. & Fung, Y. The effects of N-methyl-N-butylpyrrolidinium bis(trifluoromethylsulfonyl)imide–based electrolyte on the electrochemical performance of high capacity cathode material Li[Li0.2Mn0.54Ni0.13Co0.13]O2. *Electrochim. Acta* **59,** 14–22 (2012).
36. Martinelli, A. *et al.* Phase Behavior and Ionic Conductivity in Lithium Bis (trifluoromethanesulfonyl) imide-Doped Ionic Liquids of the Pyrrolidinium Cation and Bis (trifluoromethanesulfonyl) imide Anion. 11247–11251 (2009).
37. Zhou, Q., Henderson, W. A., Appetecchi, G. B., Montanino, M. & Passerini, S. Physical and Electrochemical Properties of N -Alkyl- N -methylpyrrolidinium Bis (fluorosulfonyl) imide Ionic Liquids : PY 13 FSI and PY 14 FSI. 13577–13580 (2008).
38. Gali, M., Lewandowski, A. & St, I. Ionic liquids as electrolytes. **51,** 5567–5580 (2006).
39. Appetecchi, G. B. *et al.* Electrochimica Acta Effect of the alkyl group on the synthesis and the electrochemical properties of N -alkyl- N -methyl-pyrrolidinium bis (trifluoromethanesulfonyl) imide ionic liquids. **54,** 1325–1332 (2009).
40. Paillard, E. *et al.* Electrochemical and Physicochemical Properties of PY 14 FSI-Based

ULSAN NATIONAL INSTITUTE OF SCIENCE AND TECHNOLOGY

Electrolytes with LiFSI. 891–895 (2009). doi:10.1149/1.3208048
41. Borgel, V., Markevich, E., Aurbach, D., Semrau, G. & Schmidt, M. On the application of ionic liquids for rechargeable Li batteries: High voltage systems. *J. Power Sources* **189,** 331–336 (2009).
42. Thackeray, M. M. *et al.* Li 2 MnO 3 -stabilized LiMO 2 (M = Mn , Ni , Co) electrodes for lithium-ion batteries {. **17,** (2007).
43. Jarvis, K. A., Deng, Z., Allard, L. F., Manthiram, A. & Ferreira, P. J. Atomic Structure of a Lithium-Rich Layered Oxide Material for Lithium-Ion Batteries : Evidence of a Solid Solution. 3614–3621 (2011).
44. Haijun Yu, H. Z. High-Energy Cathode Materials (Li2MnO3−LiMO2) for Lithium-Ion batteries. *Phys.Chem.Letter* 1268 (2013).
45. Cao, T. *et al.* Understanding the Electrochemical Properties of Li-Rich Cathode Materials from First-Principles Calculations. *J. Phys. Chem. C* **119,** 28749–28756 (2015).
46. Yabuuchi, N., Yoshii, K., Myung, S.-T., Nakai, I. & Komaba, S. Detailed Studies of a High-Capacity Electrode Material for Rechargeable Batteries, Li2MnO3−LiCo1/3Ni1/3Mn1/3O2. *J. Am. Chem. Soc.* **133,** 4404–4419 (2011).
47. Ohzuku, T., Nagayama, M., Tsuji, K. & Ariyoshi, K. High-capacity lithium insertion materials of lithium nickel manganese oxides for advanced lithium-ion batteries: toward rechargeable capacity more than 300 mA h g−1. *J. Mater. Chem.* **21,** 10179 (2011).
48. Yang, B., Li, X., Guo, H., Wang, Z. & Xiao, W. Preparation and properties of Li1.3Al0.3Ti1.7(PO4)3 by spray-drying and post-calcining method. *J. Alloys Compd.* **643,** 181–185 (2015).
49. Soo, S. *et al.* Electrochemical properties of a ceramic-polymer-composite-solid electrolyte for Li-ion batteries. *Solid State Ionics* **284,** 20–24 (2016).
50. Xu, X., Wen, Z., Wu, J. & Yang, X. Preparation and electrical properties of NASICON-type structured. **178,** 29–34 (2007).
51. Al, L. & Po, T. Preparation and characterization of lithium-ion-conductive. **425,** 103–107 (2003).
52. Kunshina, G. B., Gromov, O. G., Lokshin, E. P. & Kalinnikov, V. T. Sol – Gel Synthesis of Li 1 . 3 Al 0 . 3 Ti 1 . 7 (PO 4) 3 Solid Electrolyte. **59,** 424–430 (2014).
53. Al, L. & Po, T. Influence of Li 3 PO 4 addition on properties of. **7,** 2–6 (2011).
54. Arbi, K., Kuhn, A., Sanz, J. & García-Alvarado, F. Characterization of Lithium Insertion into NASICON-Type Li[sub 1+x]Ti[sub 2−x]Al[sub x](PO[sub 4])[sub 3] and Its Electrochemical Behavior. *J. Electrochem. Soc.* **157,** A654 (2010).
55. Li, Y. *et al.* Understanding Long-Term Cycling Performance of Li1.2Ni0.15Mn0.55Co0.1O2-Graphite Lithium-Ion Cells. *J. Electrochem. Soc.* **160,** A3006–A3019 (2013).
56. Park, K., Yu, B. & Goodenough, J. B. Li 3 N as a Cathode Additive for High-Energy-Density Lithium-Ion Batteries. 1–7 (2016). doi:10.1002/aenm.201502534
57. Park, H., Yoon, T., Kim, Y., Heon, J. & Oh, S. M. Electrochimica Acta Li 2 NiO 2 as a sacrificing positive additive for lithium-ion batteries. *Electrochim. Acta* **108,** 591–595 (2013).
58. Jin, S. *et al.* The state of understanding of the lithium-ion-battery graphite solid electrolyte interphase (SEI) and its relationship to formation cycling *. *Carbon N. Y.* **105,** 52–76 (2016).
59. Lee, Y., Choi, J., Ryou, M., Lee, Y. M. & Engineering, B. 리튬이온전지용 고분자 소재. 603–611 (2009).

ULSAN NATIONAL INSTITUTE OF
SCIENCE AND TECHNOLOGY

60. Aatiq, A., Me, M., Sik, B. M., Idriss, A. & Casablanca, B. P. On the structure of Li 3 Ti 2 (PO 4) 3. **2,**
61. Delmas, C., Nadiri, A. & Soubeyroux, J. L. The nasicon-type titanium phosphates Ati2(PO4)3 (A=Li, Na) as electrode materials. *Solid State Ionics* **28–30,** 419–423 (1988).